



On the prediction of runup, setup and swash on beaches

Paula Gomes da Silva^{a,*}, Giovanni Coco^b, Roland Garnier^c, Antonio H.F. Klein^a



^a Coastal Oceanography Laboratory, Federal University of Santa Catarina, Campus Trindade, CP 88040-900, Florianópolis, Brazil

^b School of Environment, Faculty of Science, University of Auckland, New Zealand

^c AZTI, Marine Research Division, 20110 Pasai, Spain

ARTICLE INFO

Keywords:

Swash
Setup
Nearshore bathymetry
Runup
Empirical predictors

ABSTRACT

Wave runup is one of the most critical parameters contributing to coastline flooding and shoreline change. Many formulas have been developed to empirically predict wave runup characteristics. However, large errors are still associated to these estimates, feeding a debate on the best approach to describe runup through simple parameterizations. In this work we present a comprehensive review on runup, setup and swash empirical models. We use a large database of field measurements to verify the predictive capability of recent formulas, addressing possible sources of variability. We identify the effect of the nearshore bathymetry as an important factor missing in empirical predictors and examine this issue through an analysis of runup simulated with the SWASH model over different barred and linear bathymetries. The details of the submerged beach profile affect estimates, especially with respect to setup values. The lack of standardization in measuring, post-processing and sharing runup data, limits the application of previous published databases on new analysis. We list a set of recommendations that can be used as guidelines for new measurements to broaden the applicability of the datasets in future studies. Finally, we discuss the remaining questions that still need to be further explored.

1. Introduction

Predicting wave runup (R), defined as the maximum elevation of shoreline oscillations caused by waves, has been a subject of great interest to coastal engineers and coastal managers. Runup is an important component of coastal flooding, especially during extreme storm events when energetic waves are combined with high tidal and surge levels (Alegria-Arzaburu and Masselink, 2010; Coco et al., 2014; Gomes da Silva et al., 2016; Tomás et al., 2016). Runup also plays an essential role in sediment transport, connecting the sub-aerial and submerged beach profile (e.g. Butt and Russell, 2000; Elfrink and Baldock, 2002).

The main factors affecting runup values are related to the processes occurring in the surf zone. The breaking process dissipates part of the wave energy and, at the same time, generates an additional elevation of the mean water level at the shoreline (setup - $\bar{\eta}$) due to the transfer of wave-related momentum (Longuet-Higgins and Stewart, 1964). The energy that is not dissipated reaches the shoreline as bores and causes oscillations of the water edge around the setup, the so-called swash (S) (Miche, 1951). Setup and swash levels are then, the main components of the wave runup, and have been the focus of many studies.

Understanding wave transformation is crucial to comprehend runup behavior. However, the non-linear processes occurring across the surf and swash zones, and the continuous changes in the underwater

bathymetry, whose detailed characteristics are usually unknown, render wave transformation difficult to predict. As a result, runup and its components are frequently assessed through empirical formulas based on simple environmental parameters like the slope of the beach profile (β) and the wave height (H_0) and wave length (L_0) measured offshore (usually called deep water wave parameters, although in most studies measurements are not taken in deep waters - $depth > L_0/2$) (e.g. Nielsen and Hanslow, 1991; Stockdon et al., 2006). Compared to numerical and physical modelling, empirical formulas have the advantage of being easy to apply, allowing fast and low-cost calculation. This makes such simple formulas highly demanded in coastal studies, even nowadays when computational resources are more easily available.

Usually, runup formulas for irregular waves are presented in terms of runup statistics, like the maximum runup of the time series (R_{max}), or the runup exceeded by 2% of the waves (R_2), and these formulas are criteria often used in engineering applications. Setup in turn, is represented as the average of the water level series at the shoreline. Since different processes trigger high and low frequency oscillations, the swash is commonly analysed in terms of infragravity and incident wave frequency (S_{ig} - 0.003 Hz to 0.05 Hz and S_{inc} - 0.05 Hz to 0.5 Hz). Significant infragravity and incident swash are calculated from the swash spectra, by summing the energy at the corresponding frequencies

* Corresponding author.

E-mail address: silva.p.gomes@posgrad.ufsc.br (P. Gomes da Silva).

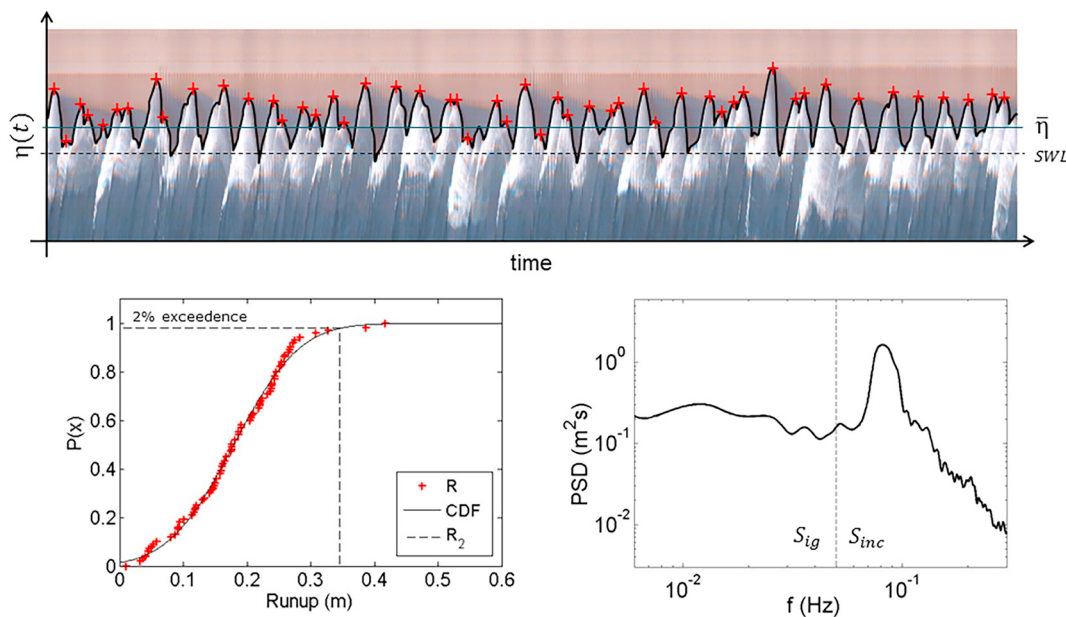


Fig. 1. a) Example of a timestack image with the digitized timeseries of shoreline motions (black thick line), the individual runup values (red pluses), and the setup level (black thin line). b) Cumulative Distribution Function of individual runups (red pluses), from which the R_2 is obtained (dashed line). c) Swash spectrum used to obtain S_{ig} and S_{inc} values – dashed line represents the limit between infragravity and incident frequencies.

(see Fig. 1).

Several field and laboratory experiments were carried out over the past decades, and many predictors have been developed. Considerable scatter still exists around the fitted equations, mainly due to errors related to processes that are important but could not be translated into simple predictors (Cox et al., 2013; Didier et al., 2016; Gomes da Silva et al., 2018; Guza and Feddersen, 2012; Poate et al., 2016; Stephens et al., 2011; Torres-Freyermuth et al., 2019). Overcoming such problems is challenging, since it is not clear which missing information is primarily responsible for those errors and how we could use it to improve runup predictions or to infer the uncertainty involved in runup estimates.

In this work we present a comprehensive review of runup, setup and swash empirical models. We compose and use a large database to verify the predictive capability of recent formulas and we discuss the sources of error involved in runup predictions. We use a numerical model to test the hypothesis that errors in runup predictions using a typical formula (Stockdon et al., 2006) are related to uncertainty in the details of the bathymetric profile.

The paper is organized as follows: Section 2 presents a detailed review on runup, swash and setup empirical formulas. Section 3 describes the methods used to evaluate the predictive capability of recent formulas and to assess the errors involved in empirical estimates. Finally, in Sections 4 and 5 we describe and discuss the results obtained, and suggest steps to move this area of research forward.

2. Empirical formulas

In this section we present a detailed review on earlier efforts to establish empirical models using data from laboratory, field experiments and numerical simulations. Fig. 2 shows a timeline of the main works that proposed parameterizations to calculate shoreline motions. Details of all equations from these works are provided in Appendix A (Table A1).

2.1. Wave reflection at the shoreline and swash saturation

The first works concerning runup prediction were presented almost seventy years ago and were mostly based on experiments with monochromatic waves. Miche (1951) hypothesized that the runup of monochromatic non-breaking waves is related to the amount of reflection at the coast. In this case, the higher the wave height, the higher the runup, resulting in the first empirical relation between the R and H_0 . For breaking waves, however, all the additional energy (above the breaking height) would be dissipated, resulting in runup saturation, which means that no increase in runup can be observed with increasing wave height.

Miche's hypothesis was tested by Guza and Bowen (1976) and later by Guza et al. (1984) using data from a laboratory planar beach. Guza et al. (1984) found that runup on beaches responds to three regimes: i) a reflective regime, when the waves are fully reflected and the runup can be calculated as the standing wave amplitude at the shoreline; ii) a saturation regime, when the waves break and the runup is not related to the wave height; and iii) an intermediate regime between the other two, obtained from the fit of their data:

$$\frac{S}{H_0} = \begin{cases} 3\xi^2/\pi & \text{if } \xi < \xi_c/3 \text{ (saturation)}, \\ (2\pi\beta)^{-0.25}\xi & \text{if } \xi_c/3 < \xi < \xi_c \text{ (transition)}, \\ (\pi/2\beta)^{0.5} & \text{if } \xi_c < \xi \text{ (reflection)}, \end{cases} \quad (1)$$

where $\xi = \beta/\sqrt{H_0/L_0}$ is the Iribarren number (Iribarren and Nogales, 1949), $\xi_c = |\pi^3/2\beta|^{0.25}$ is the critical value over which wave reflection occurs and β is the beach slope in radians (a good approximation to the tangent of the slope angle, $\tan\theta$, for all natural beaches – Holman, 1986). The saturation phenomenon, hypothesized by Miche was also verified with field measurements by Guza and Thornton (1982), who showed that the short-wave oscillations (S_{inc}) are limited by the breaking wave height, while no saturation was observed for S_{ig} .

Saturation and reflection can be associated to the beach morphodynamic state, so that on dissipative beaches, where breaking processes are dominant, the short waves energy is dissipated and the swash zone is dominated by infragravity frequencies, while on reflective beaches the runup is mainly dominated by oscillations at incident wave

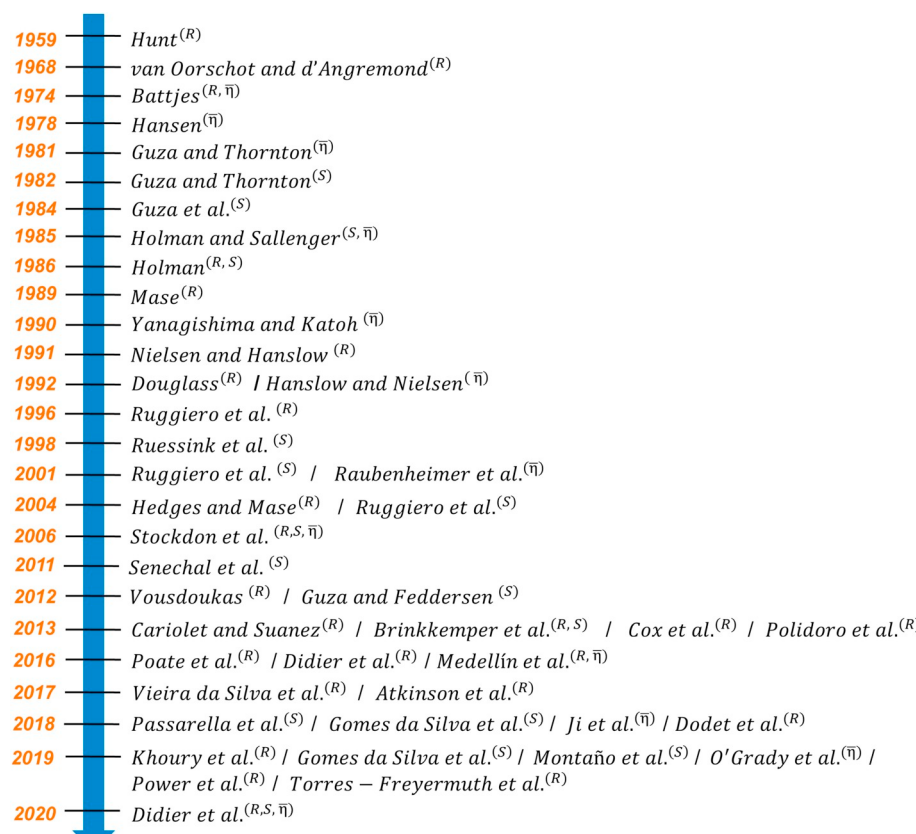


Fig. 2. Timeline with the main works that presented a parameterization of runup, setup and swash on sandy beaches. Super-indices R, S and $\bar{\eta}$ indicate the works that focused on runup, swash and setup predictions, respectively.

frequencies (Wright et al., 1985). Gomes da Silva et al. (2019), adapted the three regimes presented by Guza et al. (1984) to describe the incident swash measured on natural beaches, providing different formulas to estimate S_{inc} according to the beach state $\bar{\Omega}$ (with $\bar{\Omega}$ calculated as suggested by Wright et al., 1985):

$$\frac{S_{inc}}{H_0} = \begin{cases} 2.83\beta_s^{2.12}(H_0/L_0)^{-0.82} \text{ dissipative: } \bar{\Omega} > 5.5, \\ 0.15\beta_s^{0.56}(H_0/L_0)^{-0.64} \text{ intermediate: } 1.5 < \bar{\Omega} \leq 5.5, \\ 0.50\beta_s^{-0.37}(H_0/L_0)^{-0.15} \text{ reflective: } \bar{\Omega} \leq 1.5. \end{cases} \quad (2)$$

where β_s is slope of the swash zone (foreshore slope).

During highly dissipative conditions, however, the saturation can extend to lower frequencies. This phenomenon was observed in low sloping beaches ($0.005 \leq \beta_s \leq 0.03$), for example, by Ruessink et al. (1998) and Ruggiero et al. (2004), when studying highly dissipative conditions at Terschelling (Netherlands) and Oregon (USA), respectively. Saturation of long waves may indicate that part of the infragravity energy is dissipated or transferred to higher frequencies at surf and swash zones. Senechal et al. (2011) Eq. (3) and Eq. (4) and Brinkkemper et al. (2013) (Eq. (5) and Eq. (6)) also observed signs of such phenomenon during extreme storm events. Those authors suggested a predictor involving a hyperbolic tangent to describe swash values under saturated conditions, although both works showed different coefficients:

$$S = 2.14 \tanh(0.4H_0), \quad (3)$$

$$S_{ig} = 2.04 \tanh(0.36H_0), \quad (4)$$

$$S = 1.62 \tanh(0.5H_0), \quad (5)$$

$$S_{ig} = 1.40 \tanh(0.37H_0). \quad (6)$$

2.2. Iribarren number

Hunt (1959) studied wave-driven runup on sloped impermeable structures and proposed a direct empirical relation between the wave runup of monochromatic waves and the Iribarren number:

$$\frac{R}{H_0} = K\xi \text{ or } R = K\beta(H_0L_0)^{0.5} \quad (7)$$

where K is a constant (equals to 2.3 for average waves and 3.0 for storm conditions) and ξ is the Iribarren number, which is commonly associated to the breaking type and somehow represents the amount of energy dissipated before reaching the coast.

Most runup parameterizations are based on Hunt's equation, which was extended to natural beaches using ξ_0 , the Iribarren number calculated with offshore wave parameters (e.g. Holman, 1986; Holman and Sallenger, 1985), and ξ_b , the Iribarren number calculated with the breaking wave height (e.g. Khouri et al., 2019; Vieira da Silva et al., 2017). The first examples of the application of Hunt's formula to natural beaches are the works presented by Holman and Sallenger (1985) and Holman (1986). The authors tested the relation between ξ_0 (calculated with the slope of the swash zone β_s) and the normalized values of runup (Eq. (8)), setup and swash.

$$\frac{R_2}{H_0} = 0.20 + 0.83\xi_0. \quad (8)$$

Later, Stockdon et al. (2006) compiled data from 10 experiments carried out on east and west coast of US and in Netherlands. Measurements included a variety of beach characteristics and wave and swash conditions ($0.07 < \xi_0 < 3.25$). The dataset included R_2 , $\bar{\eta}$, S , S_{inc} , S_{ig} , H_0 , L_0 and β_s and, based on those data, they proposed the currently most accepted formula to calculate R_2 . They started from a general R_2 formula that included wave setup, infragravity and

incident swash (Eq. (9)). They then established different formulas to calculate $\bar{\eta}$, S_{ig} and S_{inc} , all based on Hunt's scaling (Eq. (10) to Eq. (12)). They also recognized the difference of swash behaviour under dissipative conditions and proposed an alternative equation to calculate wave runup (Eq. 13):

$$R_2 = \alpha \left[\bar{\eta} + \frac{\sqrt{S_{ig}^2 + S_{inc}^2}}{2} \right], \quad (9)$$

$$\bar{\eta} = 0.35\beta_s(H_0L_0)^{0.5}, \quad (10)$$

$$S_{ig} = 0.06(H_0L_0)^{0.5}, \quad (11)$$

$$S_{inc} = 0.75\beta_s(H_0L_0)^{0.5}, \quad (12)$$

$$R_{2d} = 0.043(H_0L_0)^{0.5}. \quad (13)$$

where R_{2d} is the runup exceeded by 2% of the waves during dissipative conditions ($\xi_0 < 0.3$) and $\alpha = 1.1$, is the slope of the regression fit between R_2 and the general relation $[\bar{\eta} + \sqrt{S_{ig}^2 + S_{inc}^2}/2]$. Holman and Sallenger (1985) and Stockdon et al. (2006) also investigated the role of tidal level on the dependence on ξ_0 . They examined data obtained at different tidal stages and observed a clear relation between the runup components and the Iribarren number during high and mid tide. However, no correlation was observed at low tide, particularly with respect to the setup component. The tidal level determines the part of the profile over which the waves propagate and, for intermediate and reflective beach profiles, more dissipative conditions tend to be observed at low tide. Consequently, at sites where the tidal range is large, the foreshore slope may not provide enough information to characterize the runup and additional information about the submerged beach profile (surf zone bathymetry) is needed. How to parameterize the cross-shore profile remains difficult and we report that no statistical improvement was obtained by Stockdon et al. (2006) when using the slope of the surf zone. The effect of tide was revisited in recent studies, which confirmed different runup behaviour at low and high tide (Atkinson et al., 2017; Guedes et al., 2013; Guedes et al., 2012; Guedes et al., 2011). To take into account tidal effects, Voudoukas et al. (2012) proposed a set of formulas to calculate R_2 following observations in a macrotidal beach located in Portugal. Some of the formulas proposed included the tidal level (η_{tide}) and the wind velocity (U) as predictors:

$$R_2 = 0.53\beta_s(H_0L_0)^{0.5} + 0.58\xi_0\sqrt{H_0^3/L_0} + 0.45, \quad (14)$$

$$R_2 = 0.503\beta_s(H_0L_0)^{0.5} + 0.878\xi_0\sqrt{H_0^3/L_0} - 0.016U + 0.188\eta_{tide} + 0.457. \quad (15)$$

Atkinson et al. (2017), tested formulas presented in earlier works using data from 11 different beaches along south-east Australian coast and found that site-specific condition for which the formulas were proposed were still too limited. They proposed two formulas that resulted in similar predictive skill and that were defined "model of models" (Eq. (16) and Eq. (17)), based on the predictions of all field-derived runup models (within the range of conditions they were based). The first formula (Eq. (16)) is simpler and does not differentiate the wave/morphology controls on swash and setup. The second (Eq. (17)) is more complex and include a term that represents the elevation due to the wave setup, which is in turn a function of the wave height. In both cases, runup is forced to zero when the wave energy is null:

$$R_2 = 0.99\beta_s\sqrt{H_0L_0}, \quad (16)$$

$$R_2 = 0.92\beta_s\sqrt{H_0L_0} + 0.16H_0. \quad (17)$$

2.3. Beach slope

The role of the beach slope was investigated in many studies that questioned either the dependence on the beach slope, or which slope would be representative: if the foreshore, surf zone or the average of the whole cross-shore gradient. The beach slope used in parameterizations should account for the whole history of wave transformation, from surf to swash zone. However, for pragmatic reasons, the foreshore slope is the most widely used. Nielsen and Hanslow (1991) used data measured at six beaches along the Australian coast to establish a relationship between the runup distribution and Hunt's scaling using the slope of the swash zone and the offshore wave height. They found different runup behaviour according to the beach characteristics and proposed two main formulas to be applied on beaches with different slope (Eq. (18)). Besides, according to their study, runup on milder beaches ($\beta_s < 0.1$) is a function of the wave height and wavelength only, and no relation was found with β_s :

$$R_2 = \begin{cases} 1.0005 \beta_s (H_0L_0)^{0.5} & \text{for } \beta_s \geq 0.1, \\ 0.0834 (H_0L_0)^{0.5} & \text{for } \beta_s < 0.1. \end{cases} \quad (18)$$

Ruessink et al. (1998) analysed infragravity swash from Terschelling beach (Netherlands). They tested different predictors and found a best fit correlation between the S_{ig} and H_0 , although their data also indicated that S_{ig}/H_0 depends on ξ_0 , which is calculated with β_s . Ruggiero et al. (2001), in turn, used data from the Agate (dissipative) and Duck (reflective) (USA) and found that R_2 can be estimated using only the wave height. However, a general parameterization of both datasets was possible only when the square root of β_s was included (Eq. (19)). The same predictor was used by Medellín et al. (2016) for R_2 (Eq. (20)) while the wave setup was better described by the typical Iribarren-derived relation in their data (Eq. (21)). Gomes da Silva et al. (2018) found good correlation between S_{ig} and a predictor that include the square root of the foreshore slope (Eq. (22)). Also, they showed that information about the beach state could improve the skill of the predictor:

$$R_2 = 0.27(\beta_s H_0 L_0)^{0.5}, \quad (19)$$

$$R_2 = 0.189(\beta_s H_0 L_0)^{0.5}, \quad (20)$$

$$\bar{\eta} = 0.155\beta_s(H_0L_0)^{0.5}, \quad (21)$$

$$S_{ig} = (0.19 + 0.008\bar{\Omega})(\beta_s H_0 L_0)^{0.5}. \quad (22)$$

Cariolet and Suanez (2013) used a different approach and proposed a formula to calculate R_{max} in a macrotidal beach using the slope of the "active section" of the profile, which corresponds to the section where the greatest morphological changes are observed.

2.4. Surf zone parameters

Cohn and Ruggiero (2016) investigated the effect of the variability of nearshore morphology (such as subtidal sandbars) on runup and its components on dissipative barred beaches. Using numerical experiments characterized by different measured and simulated barred profiles, they found that the nearshore bathymetry has important effect during energetic conditions, controlling up to 40% of setup, swash and runup variability. While most runup empirical models already account for the morphologic control of the subaerial beach profile (usually through β_s), the use of parameters that describe subtidal morphology still needs further attention. However, defining the ideal parameter to describe subtidal morphology is complicated, especially when multiple sandbars are present. Stockdon et al. (2006) tested predictors that included surf zone parameters (surf zone slope and breaking wave height), although no improvement was observed in runup estimates for

their dataset. Cohn and Ruggiero (2016) verified that, despite an observed large variability in nearshore bathymetry, the surf zone slope remained nearly constant and therefore did not improve linear fits. Vieira da Silva et al. (2017) used a dataset measured in Piçarras beach (Brazil) to verify the relation between different runup statistics and the Iribarren number calculated with the breaking wave height (H_b). Senechal et al. (2018) also found significant correlation between runup (total, infragravity and incident runup) and wave height measured inside the surf zone (with R^2 around 0.48). A similar study was later presented by Khoury et al. (2019). They used data from laboratory experiments to show that the relative R_{max} is better represented by the Iribarren number using the surf slope (β_{sz}) and H_b , named ξ_{sb} . Blenkinsopp et al. (2016), in turn, showed that R_2 from laboratory experiments scales well with the height of the bore collapse. Cox et al. (2013) verified the effect of the submerged profile on the infragravity swash on barred beaches and proposed a parameterization that includes the shape of the bars. Overall, the use of surf zone parameters allows accounting for beach and wave longitudinal variations. Although inclusion of these variables may improve the predictive skill (e.g. the correlation coefficient increased more than twice when using surf zone parameters in Khoury et al., 2019), collecting such measurements remains problematic.

2.5. Shape of the wave spectra

Although the beach slope and the wave parameters explain a significant part of the runup, wave breaking is not the only factor affecting the evolution of the wave energy across the profile, especially under non-monochromatic conditions. van Oorschot and D'Angremont (1968) investigated the applicability of Hunt's formula to irregular waves using laboratory data and verified that the spectral shape is relevant, and K (in Eq. (7)) is actually a function of the spectral width. The shape of the wave spectra is related to presence of groups and infragravity energy nearshore and, thus, affects swash oscillations. Almeida et al. (2017), for example, simulated an extreme event observed on a gravel barrier in South England, and compared the results from unimodal and bimodal input spectra. They verified that, when the offshore wave spectrum has a bimodal shape, short wave transformation causes the lower frequency peak to dominate, leading to larger runup excursion than it is achieved under unimodal conditions. Different spectral shapes (different broadness, peakedness and number of modal peaks) can result in the same significant wave height and peak period, but the effect of the spectrum shape is not accounted for in empirical models. As a result, parameterizations that use the peak frequency or the related wave length may fail in cases of broad/multimodal frequency spectra (Montaño et al., 2019; Poate et al., 2016; Polidoro et al., 2014). For instance, in case of bimodal sea states with similar energy peaks, the peak period can vary drastically from hour-to-hour (alternating between both peaks), affecting the fit between measurements and estimates.

Very few works attempted to add spectral information in predictive formulas. Guza and Feddersen (2012) revived this topic and assessed the effect of directional and frequency spread (σ_θ and f_s) on infragravity swash (Eq. (23)). They used numerical modelling under idealized conditions to show that the parameter $(f_p/f_s)\sigma_\theta$ is a potential predictor to improve the skill of S_g estimates, where f_p is the peak frequency:

$$S_{ig} = \{-0.031 \ln [(f_p/f_s)\sigma_\theta] + 0.058\}(H_0 L_0)^{0.5}. \quad (23)$$

Unfortunately, none of the previous field observations described provide information on directional spread.

Ruju et al. (2019) simulated the effect of frequency spread under dissipative conditions on a planar beach. Their results indicated a direct relation between the frequency spread and the infragravity runup under moderate dissipative sea states, while an inverse relation was verified

under extremely dissipative conditions. In the last case, the authors suggested that the generation of sub-harmonics due to long wave interactions may result in dissipation of the low frequency waves under extreme dissipative conditions, reducing infragravity energy in the swash zone.

Polidoro et al. (2014) and Poate et al. (2016) proposed the use of spectral periods (estimated from different spectral moments) to account for bimodal sea states. Following the same approach, Montaño et al. (2019) discussed the role of the wave frequency spread in case of bimodal sea states and the errors related to the use of T_p instead of momentum based mean period on swash predictions. They verified an inverse relationship between swash characteristics (swash excursion and mean period) and f_s . They also proposed parameterizations to estimate swash frequency spread, swash excursion and mean wave period using incident wave conditions. Still, such relations need to be further tested under different environmental conditions before they can be generalized.

2.6. Random nature of waves

Even when dealing with the same wave spectrum, some variability on runup values can still be observed and uncertainties may arise from the random nature of wave processes. The variability of phase difference between interacting waves can affect wave processes across the surf and swash-zone. Torres-Freyermuth et al. (2019) investigated the effect of the uncertainty related to the random nature of the waves on R_2 by modelling different realizations of the same wave spectrum on a planar beach and compared it with the role of frequency spreading and bed roughness. According to their results, the random characteristics of waves have more effect on runup variability (higher standard deviations within ensembles) than the other two factors, and the variability was higher in ensembles from more dissipative conditions (lower ξ_0). They presented a formula to estimate R_2 based on the simulated ensembles and the related uncertainty (which is linked to the number of standard deviations, N_σ , in each ensembles):

$$R_2 = (1.76 \pm 0.19 N_\sigma) \beta_s (H_0 L_0)^{0.5}. \quad (24)$$

56%, 86% and 95% of their data was inside the limits of 1, 2 and 3 standard deviations and the authors considered $N = 3$ a good limit to define the uncertainty associated to random waves in runup estimates. Their formula agreed with the values from previous works carried out in wave flumes, but the slope of the regression (1.76) was larger than those verified with field data (0.99 in Eq. (16)). Such difference reflects the effect that 3D features (e.g. headlands and bars systems) have on wave dissipation. These features are often present in natural beaches but were not considered in the numerical simulations.

2.7. Machine learning predictors

Recent works took advantage of the larger databases available nowadays and proposed the use of machine learning techniques to develop runup and swash predictors. Passarella et al. (2018) applied genetic programming to a number of datasets (Guedes et al., 2013; Guedes et al., 2011; Senechal et al., 2011; Stockdon et al., 2006) and proposed predictors for total and infragravity swash (Eq. (25) and Eq. (26)):

$$S = 146.737(\beta_s)^2 + \frac{T_p H_0^2}{5.8 + 10.595 H_0^2} - 4397.838(\beta_s)^4, \quad (25)$$

$$S_{ig} = \frac{\beta_s}{0.028 + \beta_s} + \frac{(-1)}{2412.255 - 5.521 \beta_s L_0} + \frac{H_0 - 0.711}{0.465 + 173.470(H_0/L_0)}. \quad (26)$$

Power et al. (2019) compiled a different dataset and also used

genetic-programming to develop a predictor that included wave steepness, the foreshore slope and roughness ($r = 2.5D_{50}$, where D_{50} is the median sediment size).

Beuzen et al. (2019) presented an alternative approach where the uncertainty in estimates is included in runup predictions using a probabilistic machine learning technique. The authors applied the estimated values to a simple dune erosion model at Narrabeen beach and verified that their approach was able to reproduce ~85% of the observed variability in dune erosion.

Although the predictors from machine learning techniques tend to outperform existing formulas, their range of validity is limited to the range of the original datasets. This is also the case for linear regression models but the strong nonlinearity of some of the machine learning techniques renders their out-of-training applications more dangerous. Also, it is almost impossible to interpret some of these predictors physically.

2.8. Gravel beaches and rocky shores

Poate et al. (2016) addressed the problem of applying formulas developed for sandy beaches to gravel beaches. Unsatisfactory results may appear due to the fundamental differences of the hydro- and morphodynamics. For example, on gravel beaches, the steeper profile tends to maintain the reflective behaviour even under energetic conditions. Poate et al. (2016) proposed two empirical formulas to calculate R_2 on gravel beaches, using data from 6 beaches located along the south and west English coast. One of the formulas included median grain size (D_{50}) (Eq. (27)) and the spectral wave period ($T_{(m-1)m0}$), while the other used the usual parameters (Eq. (28) where T_z = mean period). Both formulas showed similar skill when applied to field data.

$$R_2 = a_1 D_{50}^{-0.15} \beta_s^{0.5} T_{m-1,0} H_0, \quad (27)$$

$$R_2 = a_2 \beta_s^{0.5} T_z H_0. \quad (28)$$

where $a_1 = 0.21$ and $a_2 = 0.49$ are dimensional constants (units $m^{0.15} s^{-1}$ and s^{-1} , respectively).

Didier et al. (2016) discussed the reduction of the wave effect during inundation of a rock shore platform, which induces higher dissipation of the wave energy when compared to sandy shores. They presented an empirical formula to calculate R_{max} in those environments:

$$R_{max} = 1.91 H_0 \xi_0 + 0.22. \quad (29)$$

Dodet et al. (2018) investigated the relation between wave runup, wave parameters and beach morphology on steep and irregular rocky beach profiles in Brittany, France. They found that, for their dataset, all runup components presented a relation with $(H_0 L_0)^{0.5}$. They adapted the formula proposed by Stockdon et al. (2006) for sandy beaches to this specific type of coasts and proposed the following relation:

$$R_2 = 0.096 (H_0 L_0)^{0.5}. \quad (30)$$

2.9. Runup in estuaries and fetch limited areas

Most runup parameterizations have been developed for open coasts with sea and swell waves (gravel, sandy and rocky coasts). The application of such formulas to fetch limited, sheltered areas has not been fully analysed. These environments are typically affected by short waves and the effect of tides is very relevant (tidal dominated beaches). For most tidal levels, the waves reach the foreshore without breaking and the energy is transferred directly to the swash. Didier et al. (2020) discussed that problem and used data from five different estuarine beaches to develop a runup parameterization for sandy, gravel and mixed sandy-gravel beaches in fetch-limited environments:

$$R_2 = 0.117 (H_0 L_0)^{0.5}. \quad (31)$$

2.10. Alongshore non-uniformity

An additional issue that needs further attention is the role of alongshore variability in hydrodynamics and morphology on runup. Often, beaches present complex bathymetry which results in alongshore non-uniformity in hydrodynamics. The presence of crescentic sandbars, rip currents, beach cusps, longshore currents and infragravity motions have been shown to affect swash zone oscillations. Ruggiero et al. (2004) showed that alongshore variability on wave runup in a dissipative beach was associated to alongshore variability of the foreshore slope. Guedes et al. (2012) investigated the role of alongshore variability of wave breaking and beach slope patterns in controlling low and high frequency swash on an intermediate beach without complex morphology (no beach cusps, rip currents or crescentic bars). In this case, runup variability was predominantly induced by alongshore changes in beach slope, although their results also indicate that variations in wave breaking must also be taken into consideration in order to best predict runup height variability. Ciriano et al. (2005) used observations at Duck (North Carolina) to demonstrate that there is a coupling in morphodynamic and hydrodynamics. They assessed the wave number-frequency spectra of swash during the beach cusp evolution and showed that longshore variations in morphology due to beach cusps can cause longshore variations in low frequency flow motions directly affecting swash zone oscillations. Bryan and Coco (2010) studied the nonlinearity in wave and swash processes at bays and horns of beach cusps and verified that the morphology increases interactions between successive runups at the steep cusp horns, possibly enhancing infragravity motions. Senechal et al. (2018) analysed data measured under stationary storm wave and tidal conditions on a beach with strong 3D bar morphology associated with a shoreline sandwave, to investigate drivers of alongshore variability in runup. Their results suggest that the strong runup variability observed (runup varied by a factor of 3 along the shoreline) was mainly controlled by the morphology of the inner surf which led to rapid modification in wave patterns over a short distance (i.e. refraction around the sand wave patterns), resulting in enhancement of the incident energy level at specific locations. All these works underscore the huge complexity of 3D processes on beaches and their potential control on alongshore variability in runup. To complicate things further, one may add the effect of tides which affect/modulate the importance of 3D processes (García-Medina et al., 2020; Guedes et al., 2012, 2011). Researchers still struggle to understand how beach morphology affects runup and a predictor describing the alongshore variability control on runup remains a challenge.

2.11. Wave setup

In parallel to the works described above, several studies (besides Holman and Sallenger, 1985 and Stockdon et al., 2006) tried to establish empirical predictors to quantify wave setup. We will describe the formulas proposed in some of these studies, but a deep review on setup processes, measurement and formulations can be found in Dean and Walton (2009). The first studies on wave setup verified that the setup level at the shoreline is proportional to the offshore significant wave height. The relation was verified with data from many field experiments (Battjes, 1974; Guza and Thornton, 1981; Hansen, 1978; Nielsen, 1988), although each of those works proposed different coefficients. Later, Yanagishima and Katoh (1990) (Eq. (32)), Hanslow and Nielsen (1992) and Hanslow and Nielsen (1993) (Eq. (33)), showed an improvement in the predictive capability when adding the wavelength to setup equations.

Table 1

Available information and environmental conditions of the dataset used in the analysis.

Paper	^a N	Available data								Range of conditions		
		R ₂	$\bar{\eta}$	S	S _{ig}	S _{inc}	H ₀	L ₀	β_s	D50	^b ξ_0	^c TR
Stockdon et al. (2006)	491	x	x	x	x	x	x	x	x	X	0.07 < ξ_0 < 3.55	0.7–3.0 m
Senechal et al. (2011)	88	–	–	x	x	–	x	x	x	X	0.52 < ξ_0 < 0.88	1.5–5.0 m
Guedes et al. (2011)	25	–	–	x	x	x	x	x	x	X	1.36 < ξ_0 < 2.23	1.2–2.0 m
Guedes et al. (2013)	32	–	–	x	x	x	x	x	x	X	0.12 < ξ_0 < 0.47	1.5–3.0 m
Gomes da Silva et al. (2019, 2018)	42	x	x	x	x	x	x	x	x	X	0.71 < ξ_0 < 2.92	3.0–5.0 m
Power et al. (2019)	88	x	–	–	–	–	x	x	x	X	0.49 < ξ_0 < 2.14	0.3–5.0 m

^a N = sample size^b Estimates using $\xi_0 = \beta_s / \sqrt{H_0/L_0}$, where $L_0 = 1.56T_p^2$ ^c Typical tidal range at the experiments site.

$$\bar{\eta} = 0.052H_0 \left(\frac{H_0}{L_0} \right)^{-0.2}, \quad (32)$$

$$\bar{\eta} = 0.04(H_0 L_0)^{0.5}. \quad (33)$$

Recently, Ji et al. (2018) presented a study on the role of different beach and wave parameters on wave setup, using a coupled wave-current model over a linear bathymetry. Their results showed that wave setup is also related to wave steepness and beach slope (Eq. (34)):

$$\bar{\eta} = 0.22(\beta_s)^{0.538} H_0 \left(\frac{H_0}{L_0} \right)^{-0.371}. \quad (34)$$

The role of the beach profile and the nearshore bathymetry in runup and swash predictions was also examined in setup studies. Setup and set-down are induced to balance the cross-shore gradient of onshore momentum flux, the wave radiation stress, $-S_{xx}$. It is, therefore, expected that setup values are strongly influenced by parameters that reflect the shape of the submerged beach profile. Guza and Thornton (1981) used data from field measurements and found a relation between $\bar{\eta}$ and H_0 . They stated that the relation found between the setup and the wave height could be different on beaches with different porosity or with more complex bar structure, which could alter the spatial variation of the radiation stress.

Dean and Walton (2009) showed that the profile slope can significantly alter setup predictions. The result was confirmed and extended by Stephens et al. (2011), who tested the effect of the bar shape (e.g. bar slope, bar depth) on setup values and found significant differences when waves propagate over barred profiles with different shapes (under the same wave conditions, differences up to 100% due to changes in the bar shape were observed). Raubenheimer et al. (2001) used dataset collected at Duck (NC) to show that the setup of barred beaches is related to the average slope of the surf zone rather than to the foreshore slope:

$$\bar{\eta}/H_0 = 0.019 + 0.003(\beta_{xz})^{-1}. \quad (35)$$

Recently, O'Grady et al. (2019) used the data from Stockdon et al. (2006) to assess the role of the wave height, the beach slope and the wave steepness on setup values, by testing different empirical relations. They found that the offshore wave height explains the largest portion of the variance in setup (H_0 explained 30% in their dataset), followed by the beach slope (an improvement of 12% was obtained when β_s was added to the relation) and by the wave steepness (an improvement of 11% when $(H_0/L_0)^{-0.3}$ was added to the relation). They finally obtained the best fit with Eq. (36).

$$\bar{\eta} = 0.92\beta_s H_0 \left(\frac{H_0}{L_0} \right)^{-0.3}. \quad (36)$$

The authors stated that the variance not explained by those

parameters, could be accounted for by the errors in camera and water level measurements, the effect of local sea and remote swell (bimodal conditions), wave direction, embayment characteristics, beach porosity and water table.

2.12. Main conclusions from the review on runup, swash and setup formulas

Huge effort was made to develop and improve wave runup, swash and setup empirical predictors. A variety of approaches have been considered, different variables included and a number of observations have been used to test models. Despite improvements, errors in estimates can still be large. The Iribarren number is the basis for most of the empirical models presented so far. However, it is not clear which slope should be used. The uncertainties on runup estimates are larger in datasets from more dissipative conditions, where the shape of the submerged beach profile is clearly relevant. Nevertheless, the acquisition of such information is not always an option for users and formulas are mainly built using the foreshore slope. Other issues like the role of the shape of the wave spectra, the random nature of wave interactions, the sediment grain size and surf zone parameters, have attracted less attention, although recent studies proved the relevance of these parameters for the prediction of runup.

3. Methods

Nearshore bathymetry has an important effect on swash hydrodynamics (Cohn et al., 2014; Cohn and Ruggiero, 2016; Serafin et al., 2019; Stephens et al., 2011) and errors in runup, swash and setup estimates may arise from predictors not considering the bathymetry details. Given the difficulty of obtaining such information, very few formulas use this kind of parameter. Here we analyse the effect of such lack of information. First, we use field data to test the predictive capability of previous proposed formulas. Then, using numerical modelling, the effect of nearshore bathymetry is assessed by simulating runup over different barred and non-barred profiles. The uncertainty when applying Stockdon's formulas to those cases is then investigated.

The predictive capability of recent formulas was tested using a large database of compiled field data (the largest used until now, with 766 instances). The objective was to verify the formulas presented for sandy beaches. Thus, data from laboratory, gravel beaches or rocky shores were not included in the analysis. Since Stockdon et al. (2006) outperformed previous works, in terms of generality of the datasets considered and accuracy of the predictor, the test performed here was carried out using Stockdon et al. (2006) and formulas presented afterwards. For papers providing S_{inc} and S_{ig} , the total swash S was calculated using $S = (\sqrt{S_{ig}^2 + S_{inc}^2})/2$. Finally, the analysis was limited to the parameters included in the available databases, which means that only

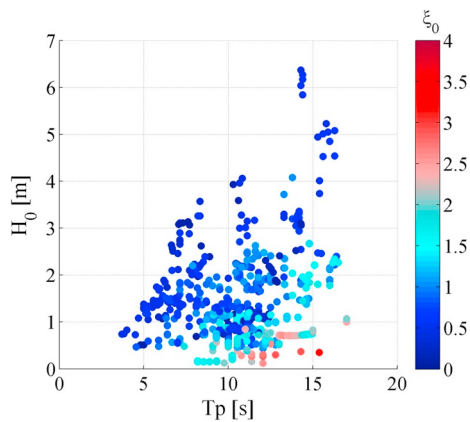


Fig. 3. Environmental conditions in the database of field measurements.

the formulas that use those available parameters, or which presented a simple way to calculate the additional parameters were tested. The formulas tested here are highlighted in bold letters in Appendix A. The skill of the formulas was based on a visual analysis of the scatter between measured and calculated data, and on the values of the coefficient of determination (the square of Pearson correlation coefficient - R^2) and the root mean square error (RMSE).

3.1. Field data

The database used to test empirical formulas was obtained from several field works published previously (Table 1). All compiled data are now available in a single database that can be accessed through the link <https://coastalhub.science/data>. Fig. 3 presents the range of conditions observed in the dataset. Measurements were taken over a variety of sea states with offshore H_0 and T_p ranging from 0.13 m to 6.37 m and from 3.7 s and 17 s, respectively, while the beach state ranged from extremely reflective (high ξ_0) to highly dissipative (low ξ_0).

3.2. Numerical simulation

To verify the effect of the nearshore (surf zone) bathymetry on runup, setup and swash predictions, several simulations were carried out using different cross-shore profile shapes. Simulations were performed employing the phase-resolving model SWASH (Simulating Waves till Shore; Zijlema et al., 2011). SWASH is based on the nonlinear shallow water equations with non-hydrostatic pressure and is suitable to simulate wave transformation in both the surf and the swash zone, accounting for the effect of wave-wave interactions, wave-current interactions, wave breaking as well as wave runup at the shoreline. We

set-up SWASH with weakly-reflective radiative boundary condition at the wavemaker. Vertical and cross-shore discretization were set with 2 layer and 1 m, respectively. Spectral parameters were used as input to obtain the short and long wave series as 1D bound waves. Nicolae Lerma et al. (2017) tested the ability of SWASH to represent swash parameters comparing simulations with observed data and found that, although the 2D model results in higher accuracy, SWASH 1D (cross-shore) represents fairly well runup and its components while it allows numerous scenarios to be simulated with low computational cost. Fiedler et al. (2019, 2018) discussed about the effect of the offshore boundary condition on runup values in simulations with the 1D SWASH, and found that the boundary assumptions of the 1D bound waves may affect offshore infragravity wave, but it does not affect runup bulk statistics, making it suitable to be used in our work. They also recommended long runs (50 min), to properly represent the infragravity swash, and Manning coefficient around 0.019. These were the settings used here.

We applied the analytical formula from (Caballeria et al., 2003) to develop barred profiles in which the geometric parameters can be modified (Eq. (37) to Eq. (41) – see parameters definition in Fig. 4). The barred bathymetry (2DV) was built using different functions for five different sections of the profile:

$$h(x) = -h_t \frac{(x - x_t)^2}{x_t^2} + h_t \text{ for } x \leq x_t, \quad (37)$$

$$h(x) = (h_c - h_t) \frac{(x - x_t)^2}{(x_m - x_t)(x_c - x_t)} + h_t; x_m = \frac{x_t + x_c}{2} \text{ for } x_t \leq x \leq x_m, \quad (38)$$

$$h(x) = (h_c - h_t) \frac{(x - x_t)^2}{(x_m - x_t)(x_c - x_t)} + h_c \text{ for } x_m < x \leq x_c, \quad (39)$$

$$h(x) = (h_f - h_c) \frac{(x - x_c)^2}{(x_f - x_c)^2} + h_c \text{ for } x_c < x \leq x_f, \quad (40)$$

$$h(x) = (h_\infty - h_f) \left\{ 1 - e^{-\frac{2[(x-x_f)(h_f-h_c)]}{[(x_f-x_c)(h_\infty-h_f)]}} \right\} + h_f \text{ for } (x_f \leq x), \quad (41)$$

where.

x_m = distance from the shoreline to the central point between the bar trough and crest;

x_c and h_c = distance and depth of the bar crest;

x_t and h_t = distance and depth of the bar trough;

x_f and h_f = distance and depth at the point offshore of the bar crest where the exponential decay of the cross-shore profile begins;

h_∞ = depth at the most offshore position.

A total of 27 single barred profiles were built by varying values of the depth of the crest h_c , the slope of the crest (β_c) and the a coefficient factor in the slope of the trough ($\beta_t = a\beta_c$) (see examples in Fig. 4). Deep water conditions were guaranteed at the most seaward position

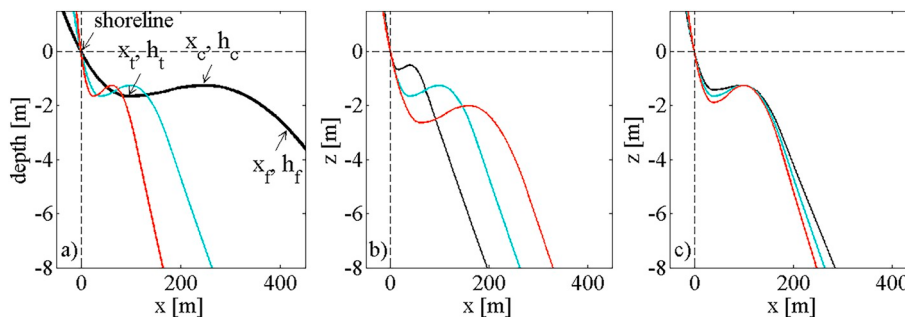


Fig. 4. Examples of barred profiles obtained by varying shape parameters like a) the slope between the shoreline and the bar crest (β_c), b) the depth of the crest (h_c) and c) the slope of the trough (through factor a).

Table 2

Values of the parameters to define the beach profile and wave conditions used in simulations with the SWASH model.

	Parameter	Values
Barred profiles	β_c	0.005; 0.0125; 0.02
	h_c (m)	0.5; 1.25; 2
	<i>a factor</i>	3; 3.5; 4
Linear profiles	β_s	0.1; 0.01
	H_0 (m)	0.5; 1; 2; 4; 6
Wave conditions	T_p (s)	6; 9; 12; 15
	ξ_0	0.5 to 3.25
Limiting to realistic conditions	H_0/L_0	< 0.04

for each profile. The parameters used in Eq. (37) to Eq. (41) were then obtained as $x_c = h_c/\beta_c$; $x_t = 0.375x_c$; $x_f = 1.75x_c$; $h_t = \beta_t x_t$ and $h_f = 0.5(x_f - x_c)\beta_b + h_c$, where the slope offshore of the bar (β_b) is defined as $\beta_b = 1.25\beta_t$. We also included two linear profiles, with β equals to 0.01 and 0.1. Different wave conditions were considered in the simulations. The values applied to generate the profiles and the range of sea states used in simulations are presented in Table 2. The barred profiles used in this section do not replicate specific measured profiles but the conditions simulated are in accordance with those verified in the field data (environmental conditions were limited to $H_0/L_0 < 0.04$, and $0.05 < \xi_0 < 3.25$) ensuring realistic simulation. Finally, a total of 484 scenarios with combinations of sea states and bathymetry were modelled. We could then explore the errors involved in the estimates of runup and its components and verify if they are a function of the shape of the bathymetry.

4. Results

4.1. Assessment of empirical formulas

Figs. 5 to 8 and Table 3 show the scatterplots between measured and calculated R_2 , S , Sig and $\bar{\eta}$ obtained from the empirical formulas, and the statistics of the performance of each one.

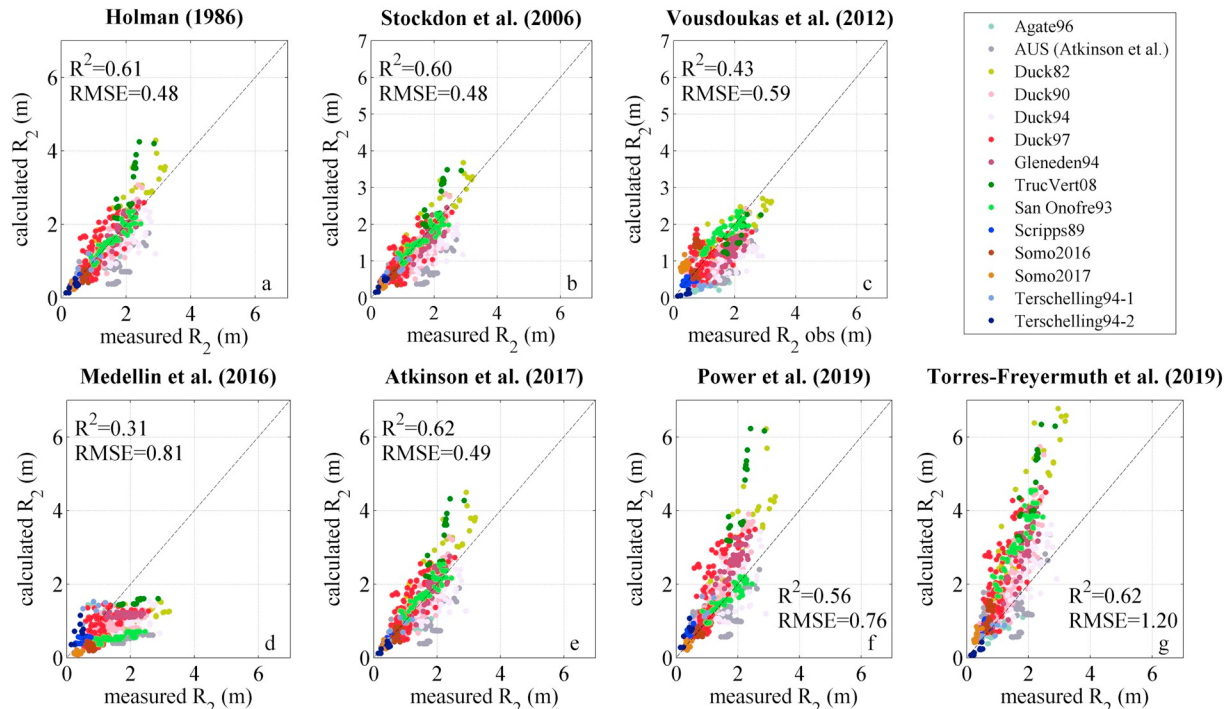


Fig. 5. Comparison of measured and predicted values of 2% runup exceedance level (R_2) using empirical formulas proposed in the literature. Different colours indicate different beach/experiments where R_2 data was available.

R_2 was initially tested using 6 formulas: Stockdon et al. (2006), Voudoukas et al. (2012), Medellín et al. (2016), Atkinson et al. (2017), Power et al. (2019) and Torres-Freyermuth et al. (2019). Atkinson et al. (2017) equation showed the best fit to measurements ($R^2 = 0.62$, RMSE = 0.49 m), followed by Stockdon et al. (2006) ($R^2 = 0.60$, RMSE = 0.48 m) (Table 3). Voudoukas et al. (2012) and Medellín et al. (2016) underestimated the majority of runup values (Fig. 5c and Fig. 5d), with most of the data distributed under the line of ideal fit and resulting in lower correlation ($R^2 = 0.43$ and $R^2 = 0.31$). Those models were based on data from one specific beach, which may explain the lower correlation ($R^2 \leq 0.43$) when they are extrapolated to other sites. Power et al. (2019), in turn, was obtained with data from many beaches (composed by sand and gravels) and laboratory data, but resulted in large overestimation of the highest runup values, and the statistics were not as good as Atkinson et al. (2017) and Stockdon et al. (2006), which used only field data. Torres-Freyermuth et al. (2019), which was based in numerical simulations on a planar beach, showed good correlation ($R^2 = 0.62$) but overestimated the runup from field data (Fig. 5g), resulting in large error (RMSE = 1.20 m). Atkinson et al. (2017) argued that, since Stockdon's model was obtained mostly based on data from one single beach (Duck, NC), simpler models such as the one presented by Holman (1986) still result in similar performance when applied to other field sites. We tested this hypothesis with the new compiled database (which includes Atkinson's and Stockdon's data) (Fig. 5a). The results indicate that in fact Holman (1986) results in similar correlation ($R^2 = 0.61$ for Holman vs $R^2 = 0.60$ for Stockdon) and RMSE (0.48 m vs 0.41 m) when compared to Stockdon et al. (2006). However, when looking at the scatterplot from both models in Fig. 5 (5a and 5b), we can see a slight overestimation of the highest values when applying Holman (1986). Atkinson et al. (2017) also seem to overestimate large runup values and the formula by Stockdon et al. (2006) still performs better under extreme conditions. Stockdon's model allows to separately estimates setup, incident and infragravity swash, which can be particularly important, given the different nature of the processes that trigger each of these components. However, some errors in the estimations of one component can be balanced by errors in other

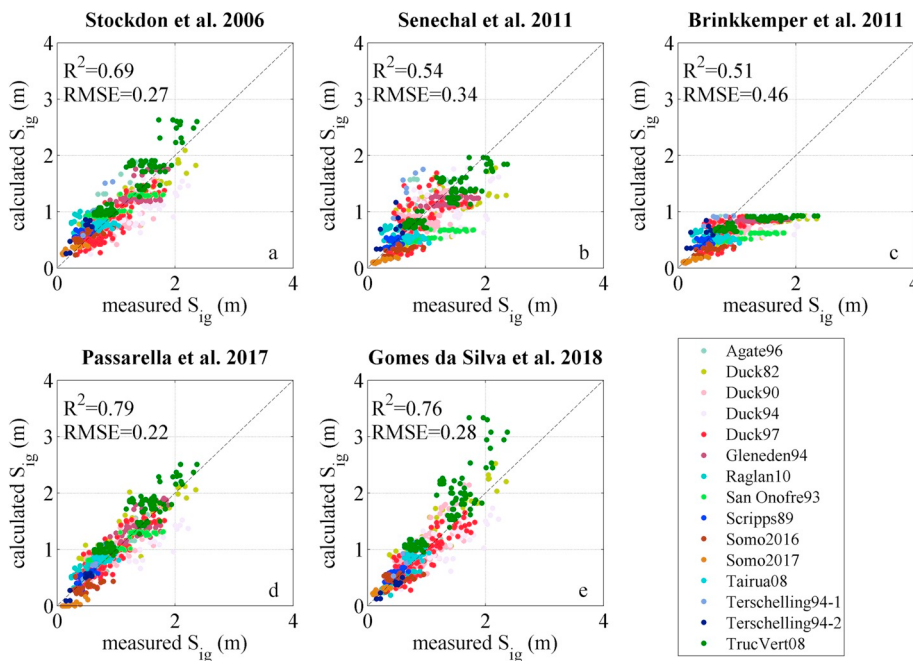


Fig. 6. Comparison between measured and calculated values of infragravity swash (S_{ig}) using empirical formulas proposed in the literature. Different colours refer to beach/experiments when S_{ig} data was available.

components, which leads to an overall good result when estimating R_2 , but lower correlation and higher errors when assessing the components separately (Stockdon et al., 2006).

The analysis of the infragravity swash calculated with the empirical formulas is presented in Fig. 6 and Table 3. The analysis was performed applying Stockdon et al. (2006), Senechal et al. (2011), Brinkkemper et al. (2013), Passarella et al. (2018) and Gomes da Silva et al. (2018). Better results were obtained from Passarella et al. (2018) followed by

Gomes da Silva et al. (2018) which showed less scatter around the ideal fit and higher R^2 (0.79 and 0.76, respectively). RMSE was 0.22 m and 0.28 m, respectively. Senechal et al. (2011) and Brinkkemper et al. (2013) were particularly focused on swash saturation during energetic conditions and used a hyperbolic tangent fit. The hyperbolic curve can lead to underestimation of runup values for unsaturated conditions (e.g. data from San Onofre beach was displaced below the ideal fit when applying both models – Fig. 6b and c). Similar results were observed for

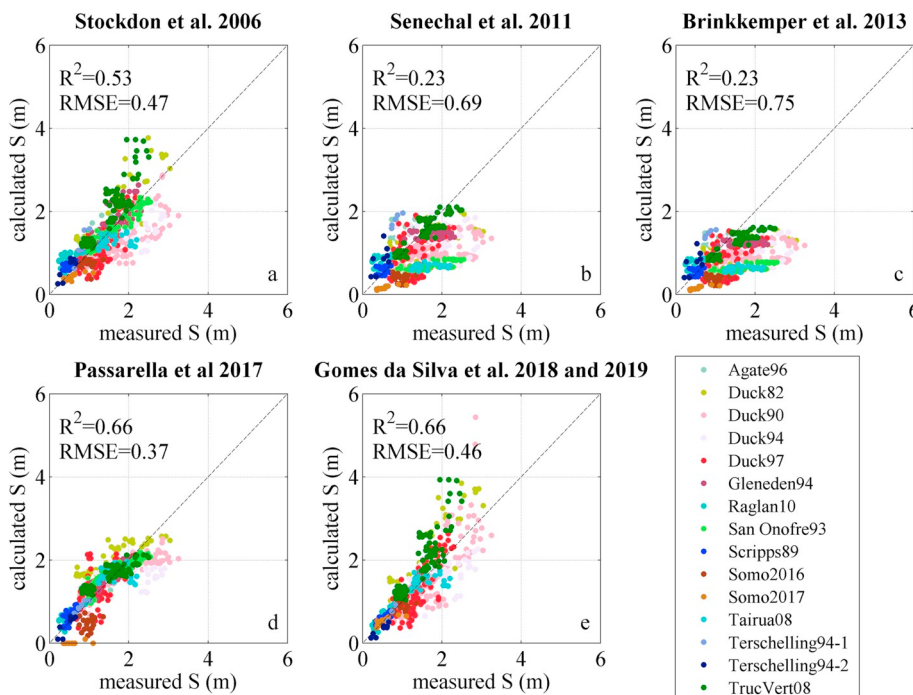


Fig. 7. Comparison between measured and calculated values of total swash (S) using empirical formulas proposed in the literature. Different colours refer to beach/experiments when swash data was available.

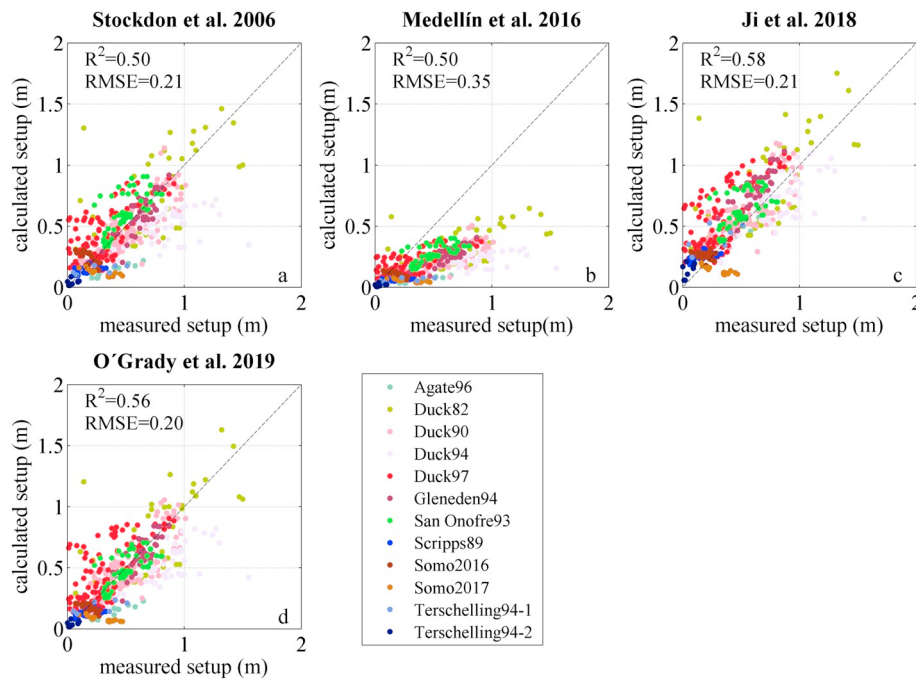


Fig. 8. Comparison between measured and calculated values of wave setup ($\bar{\eta}$) using empirical formulas proposed in the literature. Different colours refer to beach/experiments when setup data was available.

Table 3

Statistical results from the performance assessment of the empirical models. All regressions were statistically significant, with p -value $< .05$. Bold letters indicate the model that provided best results.

Predictand	Model	RMSE [m]	R ²
R_2	Holman (1986)	0.48	0.61
	Stockdon et al. (2006)	0.48	0.60
	Voudoukas et al. (2012)	0.59	0.43
	Medellín et al. (2016)	0.81	0.31
S	Atkinson et al. (2017)	0.49	0.62
	Power et al. (2019)	0.76	0.56
	Torres-Freyermuth et al. (2019)	1.20	0.62
	Stockdon et al. (2006)	0.47	0.53
S_{ig}	Senechal et al. (2011)	0.69	0.23
	Brinkkemper et al. (2013)	0.75	0.23
	Passarella et al. (2018)	0.37	0.66
	Gomes da Silva et al. (2019, 2018)	0.46	0.66
$\bar{\eta}$	Stockdon et al. (2006)	0.27	0.69
	Senechal et al. (2011)	0.34	0.54
	Brinkkemper et al. (2013)	0.46	0.51
	Passarella et al. (2018)	0.22	0.79
Fit to Stockdon's parameters	Gomes da Silva et al. (2018)	0.28	0.76
	Stockdon et al. (2006)	0.21	0.50
	Medellín et al. (2016)	0.35	0.50
	Ji et al. (2018)	0.21	0.58
O'Grady et al. (2019)			
$S_{igfit} = C_1(H_0L_0)^{0.5}$ ($C_1 = 0.06$)			
$S_{infit} = C_2\beta_s(H_0L_0)^{0.5}$ ($C_2 = 0.69$)			
$S = \sqrt{S_{igfit}^2 + S_{infit}^2}$			
$\bar{\eta}_{fit} = C_3\beta_s(H_0L_0)^{0.5}$ ($C_3 = 0.35$)			

the total swash (Fig. 7). Senechal's and Brinkkemper's models tend to follow the hyperbolic fit, underestimating extreme values. The best correlation was obtained by Passarella et al. (2018) ($R^2 = 0.66$) and Gomes da Silva et al. (2019, 2018) ($R^2 = 0.66$). The latter resulted in higher errors (RMSE = 0.46 m) in comparison to the former (RMSE = 0.37 m) and in some overestimation of the values for storm conditions (Truc Vert 2008 and Duck 1982 – Fig. 7e). The formulation presented by Passarella et al. (2018) can underestimate swash for very

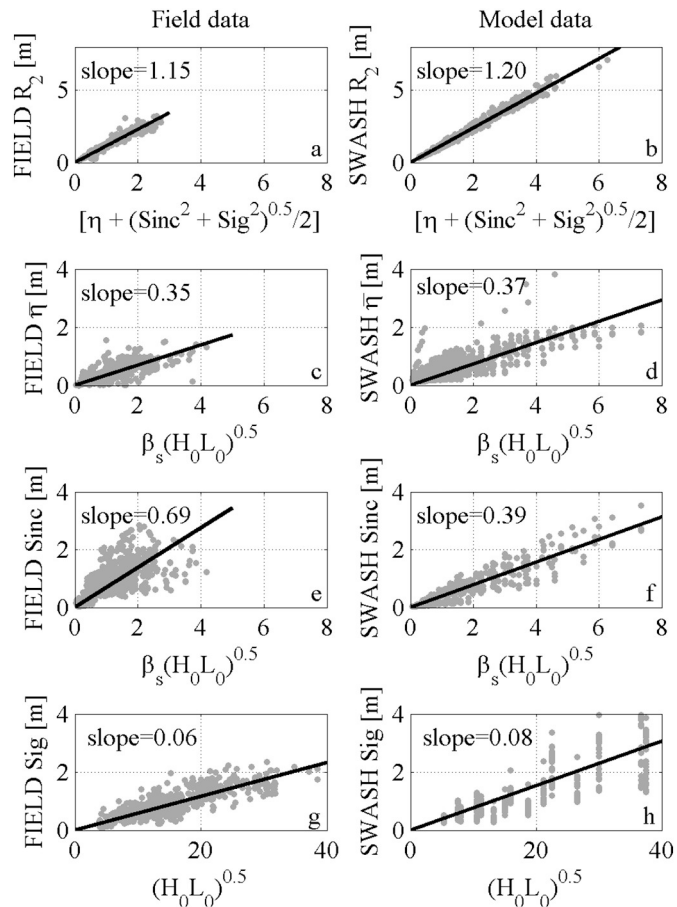


Fig. 9. Runup (a, b), setup (c, d) and swash statistics (e, f, g, h) for field data (left) and for the SWASH model (right) versus the predictive parameter used by Stockdon et al. (2006). The black line shows the best-fit.

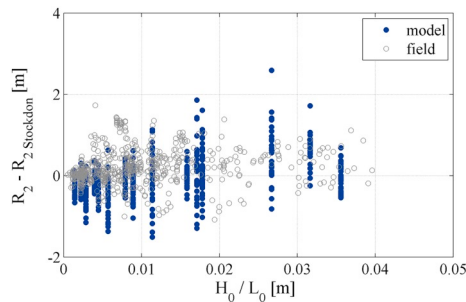


Fig. 10. Error from R_2 estimates using Stockdon parameterization on field data (R_2 measured – R_2 Stockdon) and modelled data (R_2 SWASH – R_2 Stockdon), for different sea state conditions.

low wave energy (Somo 2017 – Fig. 7d) and, since the formula has not been developed considering small values of runup, it could even result in negative predictions (here set to zero). Stockdon et al. (2006) showed an overestimation of the highest values obtained during storm conditions, such as those from Truc Vert (2008) and Duck (1982) beaches (Fig. 7a).

Finally, we tested the formulas to calculate the wave setup. Here we tested Stockdon et al. (2006), Medellín et al. (2016), Ji et al. (2018) and O'Grady et al. (2019) (Fig. 8). The higher correlation was obtained from Ji et al. (2018) (with $R^2 = 0.58$) using a model developed based on ideal scenarios (considering wave-current interactions), but that still resulted in the best setup estimates when applied to the field data used here. O'Grady et al. (2019), which was based on the dataset from Stockdon et al. (2006), showed similar results with R^2 equals to 0.56 and RMSE of 0.20 (Fig. 8d). Still, the scatter around the ideal fit is considerable for all formulas.

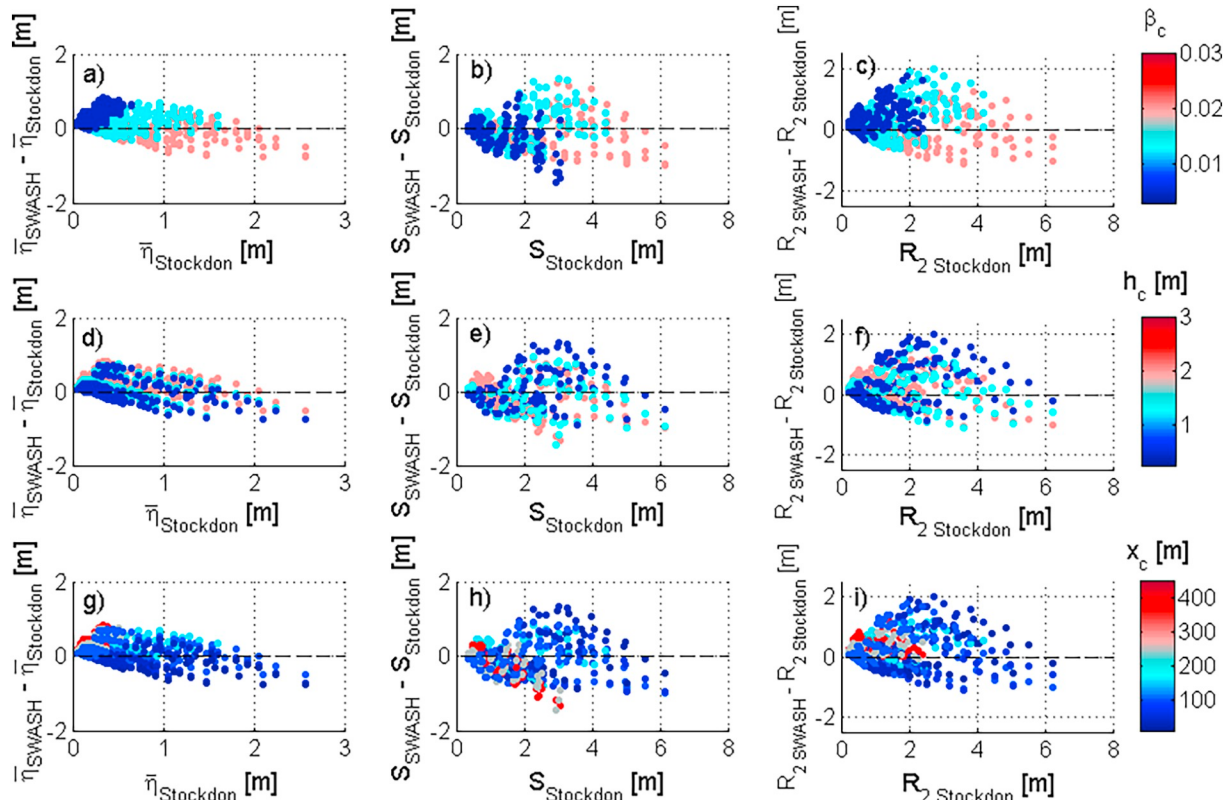


Fig. 11. Setup, swash and runup calculated with Stockdon's model vs the error obtained on estimations. The range of colours indicates the slopes of the bar crest (β_c), the bar depth (h_c) and the distance between the bar crest and the shoreline (x_c).

When fitting the parameters proposed by Stockdon et al. (2006) to the complete dataset compiled here, we observed regression coefficients similar to those from Stockdon et al. (2006) and a slight improvement in runup predictions (see fit to Stockdon's parameters in Table 3 and left panels in Fig. 9). Large errors remain in the estimation of all runup components, which indicate that we are still missing some information about the swash and setup processes that are not accounted for in current predictors.

4.2. Modelling the effect of the nearshore bathymetry

SWASH was applied to numerically-generated bathymetries to verify the effect of the cross-shore beach profile on runup estimations. Runup, setup and swash statistics (R_2 , S_{inc} , S_{tg} and $\bar{\eta}$), obtained from the model, are consistent with field observations. Parameters and coefficients obtained by Stockdon et al. (2006) can explain our modelled data (Fig. 9), supporting the use of simulated data to investigate the effect of the nearshore bathymetry. The distribution of the dataset and the slope of the regression was similar for all components (difference in coefficients less or equal to 0.05), with exception of the incident swash, which fitted to a coefficient (0.39) lower than the observed with field data (0.69). Nicolae Lerma et al. (2017) assessed the ability of SWASH (1D) to reproduce runup and its components. Their results suggest that inconsistencies in estimates may arise from complex morphology and alongshore variability in hydrodynamics, usually present in field observations and neglected in 1D cross-shore simulations. Though the application of more complex settings (i.e. 2D) would prevent us to assess the wide range of scenarios compared to the 1D model. Differences may also be due to the different definition of runup in the field observations (usually obtained from video detecting the wet/dry location) and the model (numerically, the wet/dry location corresponds to a water depth of 0.005 m) which is more evident at incident wave frequencies. Fig. 10 shows the errors observed when applying Stockdon

formula to field data (R_2 measured – R_2 Stockdon) and to the modelled data (R_2 SWASH – R_2 Stockdon). The range of sea states corresponds to those from observations, and the errors obtained from changing the shape of the bathymetry are similar to those obtained from field data.

We used simulated data to assess the effect of the bathymetric features on runup, setup and swash values. Fig. 11 shows $\bar{\eta}$, S and R_2 calculated with Stockdon et al. (2006) versus the corresponding error of those estimations. Positive and negative errors indicate underestimated and overestimated values, respectively. In general, larger runup results in higher errors (positive and negative) with residuals reaching values higher than 2 m. The colours indicate the range of the parameter of the bar shape β_c , h_c and x_c . From those parameters, the slope of the bar crest ($\beta_c = h_c/x_c$), related to the type of surf breaking, seems to be strongly related to the errors in the estimations of all runup components. The higher the slope of the sandbar, the higher the overestimation of the calculated setup, swash and consequently runup (Fig. 11a, Fig. 11b and Fig. 11c). Lower β_c , results in underestimation of the setup (blue dots over the line of zero error in Fig. 11a). The sandbar parameters can explain some of the residuals from estimations with Stockdon et al. (2006). Our analysis indicates errors in runup estimation related to the sandbar shape of the order of ± 1.5 m (Fig. 11c, f and i). The results confirm our hypothesis that the lack of information of the underwater cross-shore beach profile is a source of error in runup estimations obtained through empirical formulas.

5. Discussion

5.1. Predictive capability of recent empirical formulas

Many studies were developed in the past few years trying to explain the errors involved in runup estimations and to find an empirical formula able to reduce them. Some of the formulas used the typical parameters like the Iribarren number (e.g. Atkinson et al., 2017; Passarella et al., 2018; Senechal et al., 2011) while others included new parameters related to wave and beach characteristics (e.g. Cox et al., 2013; Gomes da Silva et al., 2018; Power et al., 2019). Usually, predictors are developed to be either more generally valid, which means that they are applicable to a wider range of conditions; or more specific, when a predictor is particularly efficient on reproducing a specific environment (Goldstein et al., 2019).

The use of additional and more complex parameters allows to explain in more detail the processes that affect swash zone oscillations and, consequently, reduce the uncertainty in estimates. On the other hand, the difficulty of measuring these new parameters may prevent users from applying such models. For example, the wave conditions used as input for the formulas refer to offshore waves characteristics (usually at 80 m depth). By using deep water wave height and length we are not accounting for the wave transformation processes, which are mainly related to site specific features (e.g. the presence of sandbars). The use of wave data measured in the surf zone, would solve that problem and allow a parameterization to be used in a greater variety of conditions possibly reducing errors. However, using the formulas would be more complicated, since users would also need to obtain wave and bathymetry data inside the surf zone. Stockdon et al. (2006) discussed this issue and concluded that, an ideal middle ground procedure would be to use wave data measured in a point located after the main wave transformation processes occur (after the influence of islands and headlands but before the wave reaches the surf zone) and deshoal it until a point offshore. This procedure neglects the surfzone and our study addressed the errors that might be associated with such hypothesis.

The performance of empirical formulas is related to the range of

conditions of the data upon which it was based. The range of the original dataset defines if the model will be general. Therefore, models based on data from very specific site and conditions (e.g. Brinkkemper et al., 2013; Medellín et al., 2016; Senechal et al., 2011; Voudoukas et al., 2012) did not perform that well for our dataset. The same is true for models which were based on dataset that included information from lab experiments and from gravel beaches. Defining a single formulation to adequately represent the runup in such large variety of conditions is clearly challenging. As a result, recent studies focusing exclusively on sandy beaches, such as Atkinson et al. (2017), Passarella et al. (2018) and Gomes da Silva et al. (2019, 2018), were able to improve the predictions of runup and its components.

Wave setup was the variable that showed the worst correlation with the predictors tested. We notice that, in contrast to other runup components, fewer studies have addressed wave setup and Stockdon et al. (2006) remains the most common predictor.

5.2. Errors in empirical estimations

Our analysis showed that missing information about the submerged beach morphology can result in large variability in runup estimates. Specifically, the distance between the shoreline and the sandbar crest (x_c), and the slope of the bar crest (β_c) affects runup estimates similar to the errors from empirical estimations. These results are in line with the findings by Raubenheimer et al. (2001) who verified that the wave setup at the shoreline is sensitive to the surf zone water depth and surf zone width, and found a strong inverse correlation between $\bar{\eta}$ and the average slope of the surf zone, $\overline{\beta_{sz}}$ ($\overline{h_{sz}}/\Delta x$), a parameter that is in some way comparable to β_c . In contrast, Cohn and Ruggiero (2016) analysed the swash dynamics in profiles with different shapes in Long Beach Peninsula (Washington coast) and found no correlation between R_{2ig} (R_2 neglecting incident swash), $\bar{\eta}$ and S_{ig} and the slope of the surf zone. However, although significant variation in bar shape was observed, variations in β_{sz} might have not been significant. Moreover, Long Beach Peninsula is typically characterized by multiple dynamical subtidal and intertidal bars, while the results showed here concerns single bar systems only. It is also possible that the parameters used to characterize single bar profiles such as β_{sz} oversimplify the process observed in more complex surf zones.

Stephens et al. (2011) used the same numerical approach applied here to verify the effect of the presence of different bar shapes on wave setup. Their results show that large variations in setup values can be observed in profiles with the same foreshore slope but different depth of the sandbar crest, which is in accordance to the results obtained from our simulations. High setup levels are usually observed at the shoreline of beaches with shallow bars (represented here by low β_c), since strong cross-shore energy gradients resulting from the abrupt energy dissipation over the bar leads to large radiations stress. The effect is enhanced if the bar is associated with steep shoaling slopes (Stephens et al., 2011). The dissipation of the wave energy over shallow bars is not accounted for in empirical formulas based on the Iribarren number, which leads to the underestimation of setup (Fig. 11a) and the overestimation of swash (Fig. 11b) observed in our results for low β_c .

Finally, it is worth noting that including information about the nearshore bathymetry in empirical formulas is a difficult task, since bathymetry data is rarely available. Some success is reported in works that have tried to fill the gap including information about beach morphodynamics in the formulas (e.g. Cariolet and Suanez, 2013; Cox et al., 2013; Gomes da Silva et al., 2019; Gomes da Silva et al., 2018), while others have proposed the use of wave parameters measured inside the surf zone (e.g. Khoury et al., 2019; Vieira da Silva et al., 2017).

5.3. Protocols for measuring, processing and sharing

The database of field measurements used here comprises a significantly broader range of conditions for sandy beaches than ever compiled before. Field data is not always made accessible to other users and, when it is, not all information needed is available. Besides, the data is not standardized. There is no protocol for measuring, post-processing and sharing the data, a fact that makes it difficult for comparisons. Here we indicate some important points to consider when planning to share measured data and facilitate uptake.

5.3.1. Wave measurements

Parameterizations are usually established using offshore wave parameters. But, as mentioned before, the relationship between runup and wave parameters measured at a single point offshore is different in exposed and sheltered shorelines. Thus, when taking measurements in sheltered areas, wave data should ideally be measured in shallow waters, after diffraction has occurred. The wave parameters can then, be deshoaled to deep waters, as suggested by Stockdon et al. (2006), Blenkinsopp et al. (2016) and Beuzen et al. (2019). Apart from wave parameters, details from the wave spectra are highly desirable as they may allow to analyse the effect of different spectral conditions. It is recommended that the full spectra, or spectral parameters (i.e. frequency and directional spreading, mean period, etc), when available, be reported.

5.3.2. Beach profile

Topographic information is used to obtain the runup level from the images (in cases of measurements through timestacks) and to calculate the beach slope. Topographic information can be obtained from a variety of methodologies such as beach survey, video images, LIDAR. Using that information, the slope of the swash zone is calculated as the slope of the profile section between the still water level and ± 2 standard deviations of the series of vertical oscillation around that level. Since the cross-shore profile is crucial for runup estimates, we recommend sharing data from the shape (and evolution) of the whole measured profile, subaerial and submerged when available. Although obtaining information about the submerged features of the beach profile is a challenge, alternatives to in-situ surveys may help improving predictions. For example, a crude estimate of the distance between the mean shoreline and the sandbar crest could be obtained through time-exposure images (averaged over a time window – typically 10 min). A typical proxy for the position of the submerged bars is the white foam generated by the wave breaking which can be easily identified in “timex” images (e.g. Holland et al., 1997; Senechal et al., 2018). Also, efforts are under way to develop algorithms capable to derive the underwater bathymetry from video images (e.g. Holman et al., 2013).

5.3.3. Runup, setup and swash

Runup measurements can be made by pressure sensors, resistance wires, video imaging, and LiDAR. All those methods were scientifically tested and showed to be valid. For measurements taken with remote techniques the resolution and related errors depend on the height and distance of the camera/LIDAR from the swash zone. When using video images, the vertical pixel resolution is typically less than 0.15 m (e.g. Gomes da Silva et al., 2018; Guedes et al., 2011; Senechal et al., 2011; Stockdon et al., 2006), while studies using LiDAR demonstrated to be valid with resolutions up to 0.03 m (Blenkinsopp et al., 2010).

R_2 , $\bar{\eta}$ and S (infragravity and incident swash) should be made available together with wave and beach parameters (foreshore slope, bar shape parameters and sediment grain size). The parameters are calculated for each burst, which usually last from 10 min to 20 min to

avoid tidal effects. Longer time series would be optimal to the study of infragravity waves and can possibly be obtained on microtidal beaches. In terms of data analysis, it is now standard practice that R_2 is calculated by fitting a density function to all runup values within the burst and estimating the runup exceeded by 2% of the waves. On the other hand, wave setup is estimated as the mean level of the series of vertical shoreline displacement (vertical value above the still water level). This implies knowing the still water level which must be acquired from equipment installed outside of the surf zones in a way that neither setup, nor setdown are part of the signal. This is probably a key factor limiting the available datasets to study wave setup. The estimation from video of both wave runup and setup as the average of the shoreline time series is limited by the fact that the point of backwash is not always clear between subsequent waves. The wave uprush usually starts before the backwash of the previous wave is completed and the mean shoreline position is displaced landward. On the other hand, on steeper beaches, bore collapse at the shoreline may generate a bore-induced setup moving the mean shoreline location shoreward (Baldock and Holmes, 1999). Details of both processes are not considered when estimating the setup level as the mean of shoreline time series, although this standard methodology is the simplest way to estimate setup from runup measurements, and it was applied in all empirical studies presented. Finally, the swash is calculated as the significant swash height, by applying a Fourier transform to the time series of vertical shoreline oscillations. Incident and infragravity significant swash are obtained by summing the energy within the respective frequency-bands.

5.4. Perspectives

After decades of studies of wave runup and its components, there are still a number of issues to be solved to improve parametric predictors based on environmental parameters. Some advances have been made regarding the importance of sediment grain size (e.g. Poate et al., 2016), the influence of tides (e.g. Atkinson et al., 2017; Holman and Sallenger, 1985) nearshore bathymetry (e.g. Cox et al., 2013), variations due to the effect of site specific geological features on wave processes (e.g. Didier et al., 2016; Dodet et al., 2019; Vieira da Silva et al., 2017) and beach type (e.g. Gomes da Silva et al., 2019; Gomes da Silva et al., 2018). More research is needed to generalize such findings and to overcome other issues listed below.

The first point to highlight is the effect of the shape of wave spectra on runup. The incident sea-swell directional spectrum is related to the occurrence of wave groups and to nonlinear forcing of infragravity waves in shallow waters (Guza and Feddersen, 2012; Madsen et al., 1997; van Oorschot and D'Angremond, 1968). Multimodal sea states can also lead to swash values different from those observed during unimodal conditions. However, wave statistics, usually applied in runup parameterizations like significant wave height and peak period, do not account for these differences in spectral shape. Although this issue was first described decades ago (van Oorschot and D'Angremond, 1968), very few works addressed this. Guza and Feddersen (2012), for example, demonstrated that accounting for the directional and frequency spreading can reduce the scatter in predictions of low frequency runup. Still, applications of this type of relations to estimate wave runup have not been fully tested. Other studies approached this problem by using momentum based spectral periods focused on gravel (Poate et al., 2016; Polidoro et al., 2014) and sandy beaches (Montaño et al., 2019), but an extra effort is still necessary to expand the application of this approach to other sites.

Another limitation identified in the literature is the complexity of the 3D bathymetry. The one-dimensional (1D) proxy assumed by empirical formulas derived for a given beach profile, does not always

represent the real state of a beach. Some beaches can present 2D/3D features in the hydrodynamics (e.g. rip-currents) or the morphology (e.g. rhythmic morphological patterns) which can cause longshore variability of runup values (Billson et al., 2019; Senechal et al., 2018; Senechal et al., 2013). Besides, other features like the presence of multiple bar systems affect the wave dissipation and shoreline oscillations. These effects are not accounted for in present empirical estimations.

One additional process neglected in the empirical formula is related to groundwater dynamics and swash permeability. The permeability determines the amount of water that infiltrates in the sediment, the amount of energy reflected at the shoreline, and thus the runup level (Kobayashi et al., 1991). The higher the permeability, the lower the level reached by waves at the shoreline. That infiltration processes not explicitly included in existing parametric formulations can be limiting (Paprotny et al., 2014; Villarroel-Lamb et al., 2014), so further studies are necessary to understand how to include this effect in runup empirical formulas.

We should also consider the possibility that empirical parametric approaches will always be affected by uncertainty that cannot be addressed using the input variables usually available (wave period and height, beach slope). Recent studies using machine learning has resulted in more accurate predictions over existing datasets. The improvement in accuracy compared to the standard predictor (e.g. Stockdon et al., 2006) comes at the price of more complicated expressions and the risk of large errors when applied to out-of-training conditions (which should not be done). As more complicated predictors are developed and more observations are available, we suggest to update the coefficients of the Stockdon et al. (2006) formula as a reference for comparison.

Finally, regarding the morphological control played by the near-shore bathymetry, some advances can be made by applying proxies to account for submerged features and relating them to swash processes. While errors can always be expected when applying simple empirical equations to describe runup, setup and swash, knowing the uncertainty

related to the processes not considered (e.g. Torres-Freyermuth et al., 2019) may be equally useful.

6. Summary

We presented a review of the empirical models proposed to predict runup, setup and swash, and discussed how the physical processes are related to the parameters used in current formulas and emphasized possible sources of errors. After testing many recently developed predictors, it appeared evident that detailed knowledge of bathymetric details is important and should be considered to improve prediction skills. We used a widely accepted numerical model, SWASH, that well compares with a commonly used runup predictor, and show that errors in the parametric formula are the same order of magnitude as induced by bathymetric variability in model simulations. We recognize that other sources of error in the present predictors need future attention (e.g. the shape of the wave spectra) as well as the challenge of obtaining and sharing such kind of measurements.

Declaration of Competing Interest

None.

Acknowledgements

The authors are very grateful to Robert Guza for his valuable suggestions and comments on various aspects of this work. We also thank Nadia Senechal and Rafael Guedes for facilitating the dataset and for discussions on data processing. This study was financed in part by the Coordenação de Aperfeiçoamento de Pessoal de Nível Superior - Brasil (CAPES) – Finance code 001 and by Conselho Nacional de Desenvolvimento Científico e Tecnológico - Brasil (CNPq) through grant 301597/2018-9. Gomes da Silva was also supported by a grant to Giovanni Coco (GNS-Natural Hazard Platform). Available datasets can be downloaded from <https://coastalhub.science/data>.

Appendix A. Empirical formulas

Table A1
Empirical formulas proposed in the literature to estimate the wave runup, setup and swash on beaches. Bold letters indicate the models tested in this work.

Reference	Equations	Range of conditions tested	Field/lab/model
Hunt (1959)	$R/H_0 = K\xi$ or $R = K\beta(H_0 L_0)^{0.5}$ $K = 2.3$ to 3 $R/H_0 = K\xi^2 K = f(\xi)$	$0.1 < \xi < 2.3$ $0.02 < H_0/L_0 < 0.112$ $0.06 < \xi < 1.61$ $0.02 < H_0/L_0 < 0.08$ –	L
van Oorschot and D'Angremond (1968)	$\bar{\eta} = \frac{5}{16}\gamma_b H_b$ $\bar{\eta} = 0.17H_0$ $\bar{\eta} = 0.33h'_b$ $R_s (cm) = 3.48 (cm) + 0.71\overline{H}_0 (cm)$	F (sandy beaches)	a
Battjes (1974)			
Guza and Thornton (1981)			
Guza and Thornton (1982)			
Guza et al. (1984)	$\frac{S}{H_0} = \begin{cases} 3\xi^2/\pi \text{ if } \xi < \xi_c/3 \text{ (saturation)} \\ (2\beta\xi)^{-0.25} \text{ if } \xi_c/3 < \xi < \xi_c \\ (\pi/2\beta)^{0.5} \text{ if } \xi_c < \xi \text{ (reflection)} \end{cases}$ where $\xi_c = \left \frac{\pi^3}{2\beta}\right ^{0.25}$	$0.4 m < H_0 < 4.0 m$ $6 s < T_p < 16 s$ $0.07 < \beta_s < 0.2$	F (sandy beaches)
Holman and Sallenger (1985)	$S_{nc}/H_0 = -0.19 + 0.69\xi_0$ $S_g/H_0 = 0.09 + 0.53\xi_0$ $\bar{\eta}/H_0 = 0.14 + 0.35\xi_0$ high tide	$0.4 m < H_0 < 4.0 m$ $6 s < T_p < 16 s$ $0.07 < \beta_s < 0.2$	F (sandy beaches)
Holman (1986)	$\bar{\eta}/H_0 = 0.06 + 0.46\xi_0$ mid tide $R_2/H_0 = 0.20 + 0.82\xi_0$ $S_2/H_0 = 0.06 + 0.85\xi_0$	$0.03 < \xi_0 < 0.25$ $0.004 < H_0/L_0 < 0.062$ $0.005 < H_0/L_0 < 0.047$	F (sandy beaches)
Mase (1989)	$R_{max}/H_0 = 2.32\xi^{0.77}$ $R_2/H_0 = 1.86\xi^{0.71}$ $\bar{\eta} = 0.052H_0(H_0/L_0)^{-0.2}$	$\beta_s \approx 0.017$ $0.17 < \xi_0 < 2.11$ $0.008 < H_0/L_0 < 0.034$ $0.026 < \beta_s < 0.119$ $0.45 < \xi_0 < 2.6$ $0.0025 < H_0/L_0 < 0.04$	F (sandy beach)
Yanagishima and Katoh (1990)			
Nielsen and Hanslow (1991)	$R_2 = \begin{cases} 1.0005\beta_s(H_0 L_0)^{0.5} \text{ for } \beta_s \geq 0.1, \\ 0.0834(H_0 L_0)^{0.5} \text{ for } \beta_s < 0.1. \end{cases}$	$0.05 < \beta_s < 0.18$ $0.4 m < H_0 < 6.4 m$ $0.03 < \beta_s < 0.16$ $0.1 < \xi_0 < 0.5$ $0.005 < H_0/L_0 < 0.04$	F (sandy beach)
Douglass (1992)	$R_{max}/H_0 = \frac{0.12}{(H_0 L_0)^{0.5}}$	$0.01 < \beta_s < 0.055$ $0.068 < \xi_0 < 0.34$ $0.003 < H_0/L_0 < 0.035$ $0.009 < \beta_s < 0.032$ $0.1 < \xi_0 < 3.5$ $0.2m < H_0 < 5m$ $0.2m < H_0 < 2.85m$	F (sandy beach) / M
Hanslow and Nielsen (1992)	$\bar{\eta} = 0.04(H_0 L_0)^{0.5}$		
Ruggiero et al. (1996)	$R_2 = 0.5H_0 - 0.22$		
Ruessink et al. (1998)	$S_{ig} = 0.16 + 0.18H_0$ $S_{ig}/H_0 = 0.02 + 2.2\xi_0$		
Ruggiero et al. (2001)	$S_{ig} = 0.27(\beta_s H_0 L_0)^{0.5}$		
Raubenheimer et al. (2001)	$\bar{\eta}/H_0 = 0.019 + 0.003(\bar{\beta}_{xz})^{-1}$		
Hedges and Mase (2004)	$R_s/H_0 = 0.27 + 1.04\xi_0$ $S_{ig} = 0.33H_0 + 0.33$ $S_{nc} = 0.11H_0 - 0.03$	$0.013 < \xi_0 < 2.4$ $1.4m < H_0 < 4.1m$ $5s < H_0 < 17s$ $0.009 < \beta_s < 0.025$	L
Ruggiero et al. (2004)			

(continued on next page)

Table A1 (continued)

Reference	Equations	Range of conditions tested	Field/lab/model
Stockdon et al. (2006)	$R_2 = 1.1 \left[\bar{\eta} + \frac{\sqrt{S_{ig}^2 + S_{mc}^2}}{2} \right]$	$0.07 < \xi_0 < 3.55$ $0.0008 < H_0/L_0 < 0.03$ $0.01 < \beta_s < 0.16$	F (sandy beaches)
Senechal et al. (2011)	$\bar{\eta} = 0.35\beta_S(H_0L_0)^{0.5}$ $S_{ig} = 0.06(H_0L_0)^{0.5}$ $S_{mc} = 0.75\beta_S(H_0L_0)^{0.5}$ $R_{sd} = 0.043(H_0L_0)^{0.5}$ $S = 2.14 \tanh(0.4H_0)$ $S_{ig} = 2.04 \tanh(0.36H_0)$	$0.56 < \xi_0 < 0.96$ $0.009 < H_0/L_0 < 0.016$ $0.05 < \beta_s < 0.08$ $0.3 < \xi_0 < 0.88$ $0.14 m < H_0 < 3.6 m$ $2.7 s < T_p < 16.5 s$ $0.04 < \beta_s < 0.15$ $\xi_0 < 0.4$ $0.4 m < H_0 < 2.5 m$ $7.14 s < T_p < 16.6 s$ $0.02 < \beta_s < 0.04$ $0.7 m < H_0 < 5.31 m$ $6 s < T_p < 16 s$ $0.021 < \beta_s < 0.035$ $0.039 < \beta_{ds} < 0.184$ $0.013 < H_0/L_0 < 0.018$ $0.04 < \beta_s < 0.12$	F (sandy beaches)
Voudouras et al. (2012)	$R_2 = 0.53\beta_S(H_0L_0)^{0.5} + 0.58\xi_0\sqrt{H_0/L_0} + 0.45$ $R_2 = 0.503\beta_S(H_0L_0)^{0.5} + 0.878\xi_0(H_0^3/L_0)^{0.5} - 0.016U + 0.188\eta_{tide} + 0.457$	$10 m \leq (H_0L_0)^{0.5} \leq 37 m$ $1 m < H_0 < 4 m$ $8 s < T_p < 15 s$	F (sandy beaches)
Guzza and Feddersen (2012)	$S_{ig} = \{-0.013 \ln[(f_p/f_s)\alpha_l] + 0.058\}(H_0L_0)^{0.5}$	—	M
Cariolet and Suanez (2013)	$R_{max} = 0.67H_0\xi_{as}$	—	M
Brinkkemper et al. (2013)	$S = 1.62 * \tanh(0.5H_0)$ $S_{ig} = 1.40 * \tanh(0.37H_0)$ $S_{mc} = 0.93 * \tanh(0.78H_0)$	$0.2 < \xi_{lm-1,0} < 1.94$ $2 m < H_0 < 7.02 m$ $4.67 s < T_{lm-1,0} < 18.55 s$ $5.11 s < T_p < 19.55 s$ $0.08 < \xi_0 < 0.69$ $0.014 < \beta_s < 0.08$ $0.1 m < H_0 < 5 m$ $2 s < T_p < 15 s$ $\beta_s = 0.09$	F (gravel beaches)
Cox et al. (2013)	$F = \begin{cases} 0.71 \text{ no bar} \\ (h_b/h_{kB})^{0.39} \text{ with bar} \end{cases}$	—	F (rocky shore)
Polidoro et al. (2014)	$R_2 = 1.04H_0 \left(\frac{T_{m-1,0}}{T_{m,0,2}} \right)^{0.5} \xi_{m-1,0}^{-0.5} [\exp(-Q_p)]^{0.5} + (0.095H_0^{0.5}L_{m-1,0})^{0.5}$	$0.2 < \xi_{lm-1,0} < 1.94$ $2 m < H_0 < 7.02 m$ $4.67 s < T_{lm-1,0} < 18.55 s$ $5.11 s < T_p < 19.55 s$ $0.08 < \xi_0 < 0.69$ $0.014 < \beta_s < 0.08$ $0.1 m < H_0 < 5 m$ $2 s < T_p < 15 s$ $\beta_s = 0.09$	F (rocky shore)
Poate et al. (2016)	$R_2 = 0.21D_{50}^{0.15}\beta_S^{0.5}H_0T_{(m-1,0)}H_0$ $R_2 = 0.49\beta_S^{0.5}T_Z H_0$	$0.5 m < H_0 < 3 m$ $2.95 s < T_p < 17.19 s$ $0.041 < \beta_s < 0.201$ $H_0/L_0 \leq 0.14$	M
Didier et al. (2016)	$R_{max} = 1.91H_0\xi_0 + 0.22$	$0 m < H_0 < 5 m$ $0 s < T_p < 15 s$ $0 < \beta_s < 0.2$	F (sandy beaches)
Medellín et al. (2016)	$R_2 = 0.189(\beta_S H_0 L_0)^{0.5}$ $\bar{\eta} = 0.155\beta_S(H_0L_0)^{0.5}$	$0.07 < \xi_0 < 3.22$ $0.4 < H_0 < 6.4 m$ $3.7 s < T_p < 16.4 s$ $0.01 < \beta_s < 0.16$	F (sandy beaches)
Atkinson et al. (2017)	$R_2 = 0.99\beta_S(H_0L_0)^{0.5} + 0.16H_0$ $R_2 = 0.92\beta_S(H_0L_0)^{0.5} + 0.16H_0$	$0.066 < \xi_0 < 3.01$ $0.0005 < H_0/L_0 < 0.04$ $0.01 < \beta_s < 0.16$	F (sandy beaches)
Passarella et al. (2018)	$S = 146.737(\beta_S)^2 + \frac{T_p H_0^2}{5.8 + 10.595\sqrt{H_0^2}} - 4397.838(\beta_S)^4$	$0.07 < \xi_0 < 3.22$ $0.4 < H_0 < 6.4 m$ $3.7 s < T_p < 16.4 s$ $0.01 < \beta_s < 0.16$	F (sandy beaches)
Gomes da Silva et al. (2018)	$S_{ig} = \frac{\beta_S}{0.28 + \beta_S} + \frac{(-1)}{2412.255 - 5.321\beta_S L_0} + \frac{H_0 - 0.711}{0.465 + 173.470(H_0/L_0)}$ $S_{ig} = (0.19 + 0.008\bar{\Omega})(\beta_S H_0 L_0)^{0.5}$	b	(continued on next page)

Table A1 (continued)

Reference	Equations	Range of conditions tested	Field/lab/model
Ji et al. (2018)	$\bar{\eta} = 0.22(\beta_s)^{0.538} H_0 (H_0/L_0)^{-0.371}$	$0.0104 < \xi_0 < 1.408$ $0.28 m < H_0 < 4.25 m$ $2 s < T_p < 14 s$ $0.005 < \beta_s < 0.1$ $0.5 < \xi_0 < 5.5$ $0.1 < \beta_s < 0.4$ $0.2 < \xi_0 < 1$ $0.1 < \xi_{sb} < 0.7$ $0.05 < \beta_s < 0.2$ $0.02 < \beta_{ss} < 0.13$ $0.066 < \xi_0 < 3.226$ $0.009 < \beta_s < 0.2865$ $0.0002 m < D50 < 0.05 m$	M
Dodet et al. (2018)	$R_2 = 0.096(H_0 L_0)^{0.5}$		F (cliffs)/M
Khoury et al. (2019)	$\frac{R_{max}}{H_0} = 1.06 \xi_{sb} = 1.06 \frac{\beta_{ss}}{\sqrt{H_0 / L_0}}$		L
Power et al. (2019)	$\begin{aligned} R2 \% / H_0 = & (x2 + (((x3, * 3) / \exp(-5)), * ((3, * x3), * x3)) + (((x1 + x3) - 2) - \\ & (x3 - x2)) + ((x2 - x1) - x3) + (((x3, * x1) - (x3, (1/3)) - (\exp(x2), (x1, * 3))) \\ & + \sqrt{(((x3 + x1) - x2) - (x2 + \log(10(x3))) + (((x2, 2), (x1, (1/3)), \\ & (x1, (1/3))) - \sqrt{x3}) + (\sqrt{x2 + ((x3, * x1), (1/3))) + (\log(2) - (1, /1 + \exp \\ & (- (x2 + x3))) + (\sqrt{x3} - (x2, 2)) + 3, * (x2, 2)) + (((x3, * - \\ & 5), 2) + (((x3 + x3), * x1), * (x2, 2)) + \log((\sqrt{((x2, 2) + (x3, 7) / \\ & 3))) + ((x2 + 3), (1/3))) + (((x1, * x3), * (-5, 2)), * (x3, 2)) - \log(10((1, / \\ & 1 + \exp(- (x2 + x3)))) + (x1, x3) + \exp(- (((x3, /x1), \exp(4)) + (\exp \\ & (x3, * 3), 2)) + \exp(\log((x2 - x3)) - \log(\exp(- ((-1 + x1), 2)))) + ((\sqrt{ \\ & 4}, * (((x3, * x2) - x2) - (0, * x1)), 2) + (2, * ((((-5, * x3) + x1), * (2 - x3)) - \\ & 2) + ((\sqrt{4}, * (((x3, (x2) - x2) - (0 - x1)), 2) + ((((-5 + x1) - x2), * (x2 - \\ & x3)), * ((x1 - x2) - (-4, * -5)) + (\exp(-(x2 + (-5 - x1), 2)) + ((x2 + 5), * (x3, 2))) - \\ & + \sqrt{1, /1 + \exp(- (\exp(x1) - \exp(-(x3 + x3), 2))) + ((x1, x3) - \\ & (x3, * 4))), 2) + ((\exp(- (((\exp(-(- ((\sqrt{x3}, * 4) + (1, /1 + \exp \\ & (- (x2 + 2))), 2)), 2) + x1, 2)), 3) \\ where x1 = & H_0/L_0, x2 = \beta_s, x3 = r/H_0, (r = 2.5D50) \\ S_{nc} = & \begin{cases} 2.83\beta_s^{2.12}(H_0/L_0)^{-0.32} dissipative: \bar{\Omega} > 5.5 \\ 0.15\beta_s^{0.36}(H_0/L_0)^{-0.64} Intermediate: 1.5 < \bar{\Omega} \leq 5.5 \\ 0.59\beta_s^{-0.37}(H_0/L_0)^{-0.15} reflective: \bar{\Omega} \leq 1.5 \end{cases} \\ \bar{\eta} = & 0.92\beta_s H_0 (H_0/L_0)^{-0.3} \end{aligned}$	$0.066 < \xi_0 < 3.01$ $0.0005 < H_0/L_0 < 0.04$ $0.01 < \beta_s < 0.16$	F (sandy beaches)
Gomes da Silva et al. (2019)		$0.07 < \xi_0 < 3.55$ $0.0008 < H_0/L_0 < 0.03$ $0.01 < \beta_s < 0.16$ $0.28 < \xi_0 < 1.58$ $0.40 m < H_0 < 2.40 m$ $3 s < T_p < 16 s$ $0.11 < \beta_s < 0.16$ $0.3 < \xi_0 < 2.5$ $0.00023 m < D50 < 0.00011 m$	M
Torres-Freyermuth et al. (2019)	$R_2 = (1.76 \pm 0.19 N_o) \beta_s (H_0 L_0)^{0.5}$		F
Montaño et al. (2019)	$S = c (H_0 / L_0)^{0.25} f_s^2 T L c = f(\beta_s)$		
Didier et al. (2020)	$R_2 = 0.117(H_0 L_0)^{0.5}$		

^a Development from previous formulas^b Model of models fitted to a realistic range of conditions (verified with field data)^c T and L are peak or spectral momentum-based wave period and length

Appendix B. List of symbols

- β = slope of the beach profile
 β_{as} = slope of the active section of the beach profile
 β_b = slope offshore of the bar
 β_c = slope between the shoreline and the bar crest
 β_s = slope of the swash zone
 β_{sz} = slope of the surfzone
 β_t = slope between the shoreline and the bar trough
 Δx = discrete cross – shore distance
 ξ = Iribarren number
 ξ_0 = Iribarren number calculated with deep water wave parameters
 ξ_{as} = Iribarren number calculated with the slope of the active section of the profile
 ξ_b = Iribarren number calculated with breaking wave height
 ξ_c = Critical value of the Iribarren number over which reflection occurs
 ξ_{sz} = Iribarren number calculated with the slope of the surf zone
 ξ_{sb} = Iribarren number calculated with breaking wave height and surf zone slope
 $\bar{\eta}$ = wave setup
 η_{tide} = tidal level
 γ_b = empirical ratio of breaking wave height to depth
 $\bar{\Omega}$ = parameter that defines the beach morphodynamic state according to Wright et al. (1985)
 σ_θ = wave directional spread
 D_{50} = median grain size
 f_p = wave peak frequency
 f_s = wave frequency spread
 h'_b = depth of maximum radiation stress
 h_c = depth of the bar crest
 h_f = depth offshore of the bar crest where the exponential decay begins
 h_{NB} = depth that would exist should no bar be present
 $\overline{h_{sz}}$ = average depth of the surf zone
 h_t = depth of the bar trough
 h_∞ = depth in the most offshore position
 H_b = breaking wave height
 H_0 = offshore significant wave height
 L_0 = wave length in deep waters
 $L_{m-1,0}$ = wave length calculated with the spectral period $T_{m-1,0}$
 m = spectral momentum
 N_σ = number of standard deviations
 Q_p = spectral peakedness
 r = roughness

R = wave runup

R_2 = runup height exceeded by 2% of the waves

R_{2ig} = R_2 resultant from setup and infragravity swash (incident swash is neglected)

R_{2d} = R_2 in dissipative beaches

R_{max} = maximum runup

S = significant swash

S_{inc} = significant incident swash

S_{ig} = significant infragravity swash

S_2 = swash level exceeded by 2% of the waves

$T_{m0,2}$ = spectrally derived wave period ($T_{m0,2} = \sqrt{m_0/m_2}$)

$T_{m-1,0}$ = spectrally derived wave period ($T_{m-1,0} = m_{-1}/m_0$)

T_p = peak period

T_z = mean period

TR = tidal range

U = wind velocity

x_c = distance of the bar crest from the shoreline

x_f = distance from the shoreline to the point offshore of the bar crest where the exponential decay begins

x_m = distance between the shoreline and the central point between the bar trough and crest

x_t = distance between the shoreline and the bar trough

References

- Alegria-Arzaburu, A.R., Masselink, G., 2010. Storm response and beach rotation on a gravel beach, Slapton Sands, U.K. Mar. Geol. 278, 77–99. <https://doi.org/10.1016/j.margeo.2010.09.004>.
- Almeida, L.P., Masselink, G., McCall, R., Russell, P., 2017. Storm overwash of a gravel barrier: field measurements and XBeach-G modelling. Coast. Eng. 120, 22–35. <https://doi.org/10.1016/j.coastaleng.2016.11.009>.
- Atkinson, A.L., Power, H.E., Moura, T., Hammond, T., Callaghan, D.P., Baldock, T.E., 2017. Assessment of runup predictions by empirical models on non-truncated beaches on the south-east Australian coast. Coast. Eng. 119, 15–31. <https://doi.org/10.1016/j.coastaleng.2016.10.001>.
- Baldock, T.E., Holmes, P., 1999. Simulation and prediction of swash oscillations on a steep beach. Coast. Eng. 36, 219–242. [https://doi.org/10.1016/S0378-3839\(99\)00011-3](https://doi.org/10.1016/S0378-3839(99)00011-3).
- Battjes, J.A., 1974. Computation of Set-up, Longshore Currents, Run-Up and Overtopping Due to Wind-Generated Waves. Delft University of Technology.
- Beuzen, T., Goldstein, E.B., Splinter, K.D., 2019. Ensemble models from machine learning: an example of wave runup and coastal dune erosion. Nat. Hazards Earth Syst. Sci. Discuss. <https://doi.org/10.5194/nhess-2019-81>.
- Billson, O., Russell, P., Davidson, M., 2019. Storm waves at the shoreline: when and where are infragravity waves important? J. Mar. Sci. Eng. 7. <https://doi.org/10.3390/jmse7050139>.
- Blenkinsopp, C.E., Mole, M.A., Turner, I.L., Peirson, W.L., 2010. Measurements of the time-varying free-surface profile across the swash zone obtained using an industrial LIDAR. Coast. Eng. 57, 1059–1065. <https://doi.org/10.1016/j.coastaleng.2010.07.001>.
- Blenkinsopp, C.E., Matias, A., Howe, D., Castelle, B., Marie, V., Turner, I.L., 2016. Wave runup and overwash on a prototype-scale sand barrier. Coast. Eng. 113, 88–103. <https://doi.org/10.1016/j.coastaleng.2015.08.006>.
- Brinkkemper, J., Torres-Freyermuth, A., Mendoza, E.T., Ruessink, B.G., 2013. Parameterization of wave run-up on beaches in Yucatan, Mexico: a numerical study. In: Coastal Dynamics, pp. 225–234.
- Bryan, K.R., Coco, G., 2010. Observations of nonlinear runup patterns on plane and rhythmic beach morphology. Journal of Geophysical Research 115 (C09017). <https://doi.org/10.1029/2009JC005721>.
- Butt, T., Russell, P., 2000. Hydrodynamics and cross-shore sediment transport in the swash-zone of natural beaches: a review. J. Coast. Res. 16, 255–268.
- Caballeria, M., Calvete, D., Coco, G., Dodd, N., Falquen, A., 2003. Formation and alongshore spacing of crescentic bars. In: Proc. 3rd Symposium on River, Coastal and Estuarine Morphodynamics. Barcelona, Spain, pp. 310–319.
- Cariolet, J., Suarez, S., 2013. Runup estimations on a macrotidal sandy beach. Coast. Eng. 74, 11–18. <https://doi.org/10.1016/j.coastaleng.2012.11.008>.
- Ciriano, Y., Coco, G., Bryan, K.R., Elsgar, S., 2005. Field observations of swash zone infragravity motions and beach cusp evolution. Journal of Geophysical Research 110 (C02018). <https://doi.org/10.1029/2004JC002485>.
- Coco, G., Senechal, N., Rejas, A., Bryan, K.R., Capo, S., Parisot, J.P., Brown, J.A., MacMahon, J.H.M., 2014. Beach response to a sequence of extreme storms. Geomorphology 204, 493–501. <https://doi.org/10.1016/j.geomorph.2013.08.028>.
- Cohn, N., Ruggiero, P., 2016. The influence of seasonal to interannual nearshore profile variability on extreme water levels: Modeling wave runup on dissipative beaches. Coast. Eng. 115, 79–92. <https://doi.org/10.1016/j.coastaleng.2016.01.006>.
- Cohn, N., Ruggiero, P., Ortiz, J., Walstra, D.J., 2014. Investigating the role of complex sandbar morphology nearshore hydrodynamics. In: Proc. 13th International Coastal Symposium, pp. 053–058. <https://doi.org/10.2112/SI65-010.1>.
- Cox, N., Dunkin, L.M., Irish, J.L., 2013. An empirical model for infragravity swash on barred beaches. Coast. Eng. 81, 44–50. <https://doi.org/10.1016/j.coastaleng.2013.06.008>.
- Dean, B.G., Walton, T.L., 2009. Wave set-up. In: Kim, Young C. (Ed.), Handbook of Coastal and Ocean Engineering. World Scientific, pp. 21–44. https://doi.org/10.1007/978-981-481-2639-2_165.
- Didier, D., Bernatchez, P., Marie, G., Boucher-Brossard, G., 2016. Wave runup estimations on platform-beaches for coastal flood hazard assessment. Nat. Hazards 83, 1443–1467. <https://doi.org/10.1007/s11069-016-2399-5>.
- Didier, D., Caulet, C., Bandet, M., Bernatchez, P., Dumont, D., Augereau, E., Floc'h, F., Delacourt, C., 2020. Wave runup parameterization for sandy, gravel and platform beaches in a fetch-limited, large estuarine system. Cont. Shelf Res. 192, 104024. <https://doi.org/10.1016/j.csr.2019.104024>.
- Dodet, G., Leckler, F., Sous, D., Ardhuin, F., Filipot, J.F., Suarez, S., 2018. Wave runup over steep rocky cliffs. J. Geophys. Res. Ocean. 123, 7185–7205. <https://doi.org/10.1029/2018JC013967>.
- Dodet, G., Melet, A., Ardhuin, F., Bertin, X., Idier, D., Almar, R., 2019. The contribution of wind-generated waves to coastal sea-level changes. Surv. Geophys. <https://doi.org/10.1007/s10712-019-09557-5>.
- Douglass, S.L., 1992. Estimating extreme values of run-up on beaches. J. Waterw. Port Coast Ocean Eng. 118, 220–224. [https://doi.org/10.1061/\(ASCE\)0733-950X\(1992\)118:2\(220\)](https://doi.org/10.1061/(ASCE)0733-950X(1992)118:2(220)).
- Elfrink, B., Baldock, T., 2002. Hydrodynamics and sediment transport in the swash zone: a review and perspectives. Coast. Eng. 45, 149–167. [https://doi.org/10.1016/S0378-3839\(02\)00032-7](https://doi.org/10.1016/S0378-3839(02)00032-7).
- Fiedler, J.W., Smit, P.B., Brodie, K.L., McNinch, J., Guza, R.T., 2018. Numerical modeling of wave runup on steep and mildly sloping natural beaches. Coast. Eng. 131, 106–113. <https://doi.org/10.1016/j.coastaleng.2017.09.004>.
- Fiedler, J.W., Smit, P.B., Brodie, K.L., McNinch, J., Guza, R.T., 2019. The offshore boundary condition in surf zone modeling. Coast. Eng. 143, 12–20. <https://doi.org/10.1016/j.coastaleng.2019.01.001>.

- [10.1016/j.coastaleng.2018.10.014](https://doi.org/10.1016/j.coastaleng.2018.10.014).
- García-Medina, G., Ozkan-Haller, H.T., Ruggiero, P., Holman, R.A., Li, C., 2020. Runups of unusual size: roughness and variability of swash. *J. fo Geophys. Res. - Ocean*. 1–27. <https://doi.org/10.1029/2019JC015186>.
- Goldstein, E.B., Coco, G., Plant, N.G., 2019. A review of machine learning applications to coastal sediment transport and morphodynamics. *Earth-Science Rev.* 194, 97–108. <https://doi.org/10.1016/j.earscirev.2019.04.022>.
- Gomes da Silva, P., Dalinghaus, C., González, M., Gutiérrez, O., Espejo, A., Abascal, A.J., Klein, A.H.F., 2016. Estimating flooding level through the Brazilian coast using re-analysis data. *J. Coast. Res.* 1092–1096. <https://doi.org/10.2112/SI75-219.1>.
- Gomes da Silva, P., Medina, R., González, M., Garnier, R., 2018. Infragravity swash parameterization on beaches: the role of the profile shape and the morphodynamic beach state. *Coast. Eng.* 136, 41–55. <https://doi.org/10.1016/j.coastaleng.2018.02.002>.
- Gomes da Silva, P., Medina, R., González, M., Garnier, R., 2019. Wave reflection and saturation on natural beaches: the role of the morphodynamic beach state in incident swash. *Coast. Eng.* 153, 103540. <https://doi.org/10.1016/j.coastaleng.2019.103540>.
- Guedes, R.M.C., Bryan, K.R., Coco, G., Holman, R.A., 2011. The effects of tides on swash statistics on an intermediate beach. *J. Geophys. Res.* 116. <https://doi.org/10.1029/2010JC006660>.
- Guedes, R.M.C., Bryan, K.R., Coco, G., 2012. Observations of alongshore variability of swash motions on an intermediate beach. *Cont. Shelf Res.* 48, 61–74. <https://doi.org/10.1016/j.csr.2012.08.022>.
- Guedes, R.M.C., Bryan, K.R., Coco, G., 2013. Observations of wave energy fluxes and swash motions on a low-sloping, dissipative beach. *J. Geophys. Res. Ocean*. 118, 3651–3669. <https://doi.org/10.1002/jgrc.20267>.
- Guza, R.T., Bowen, A.J., 1976. Resonant interactions for waves breaking on a beach. In: Proc. 15th International Conference on Coastal Engineering. Honolulu, Hawaii, pp. 560–579. <https://doi.org/10.1061/9780872620834.032>.
- Guza, R., Feddersen, F., 2012. Effect of wave frequency and directional spread on shoreline runup. *Geophys. Res. Lett.* 39. <https://doi.org/10.1029/2012GL051959>.
- Guza, R.T., Thornton, E.B., 1981. Wave set-up on a natural beach. *J. Geophys. Res.* 86, 4133–4137. <https://doi.org/10.1029/JC086iC05p04133>.
- Guza, R.T., Thornton, E.B., 1982. Swash oscillations on a natural beach. *J. Geophys. Res.* 87, 483–491. <https://doi.org/10.1029/JC087iC01p00483>.
- Guza, R.T., Thornton, E.B., Holman, R.A., 1984. Swash on steep and shallow beaches, in: Proc. In: 19th International Conference on Coastal Engineering. Houston, Texas, pp. 708–723. <https://doi.org/10.9753/icce.v19.48>.
- Hansen, U.A., 1978. Wave setup and design water level. *J. Waterw. Port Coast Ocean Eng.* 104, 227–240.
- Hanslow, D.J., Nielsen, P., 1992. Wave setup on beaches and in river entrances. In: Proc. of the 23rd International Conference on Coastal Engineering. Venice, Italy, pp. 240–252. <https://doi.org/10.9753/icce.v23.%25p>.
- Hanslow, D.J., Nielsen, P., 1993. Shoreline set-up on natural beaches. *J. Coast. Res. SI*. <https://doi.org/10.1061/9780872629332.018>.
- Hedges, T.S., Mase, H., 2004. Modified Hunt's equation incorporating wave setup. *J. Waterw. Port Coast Ocean Eng.* 130, 109–113. [https://doi.org/10.1061/\(ASCE\)0733-950X\(2004\)130:3\(109\)](https://doi.org/10.1061/(ASCE)0733-950X(2004)130:3(109)).
- Holland, K.T., Holman, R.A., Lippman, T.C., Stanley, J., 1997. Practical use of video imagery in nearshore oceanographic field studies. *Journal of Oceanic Engineering* 22 (1). <https://doi.org/10.1109/48.557542>.
- Holman, R.A., 1986. Extreme value statistics for wave run-up on a natural beach. *Coast. Eng.* 9, 527–544. [https://doi.org/10.1016/0378-3839\(86\)90002-5](https://doi.org/10.1016/0378-3839(86)90002-5).
- Holman, R.A., Sallenger, A.H., 1985. Setup and swash on a natural beach. *J. Geophys. Res.* 90, 945–953. <https://doi.org/10.1029/JC090iC01p000945>.
- Holman, R., Plant, N., Holland, T., 2013. CBathy: a robust algorithm for estimating nearshore bathymetry. *J. Geophys. Res. Ocean*. 118, 2595–2609. <https://doi.org/10.1029/jgrc.2019>.
- Hunt, I.A., 1959. Design of sea walls and breakwaters. *J. Waterw. Port Ocean Eng.* 85 (123), 152.
- Iribarren, R., Nogales, C., 1949. Protection of ports. In: PIANC World Congress, pp. 31 Lisbon.
- Ji, C., Zhang, Q., Wu, Y., 2018. An empirical formula for maximum wave setup based on a coupled wave-current model. *Ocean Eng.* 147, 215–226. <https://doi.org/10.1016/j.oceaneng.2017.10.021>.
- Khoury, A., Jarno, A., Marin, F., 2019. Experimental study of runup for sandy beaches under waves and tide. *Coast. Eng.* 144, 33–46. <https://doi.org/10.1016/j.coastaleng.2018.12.003>.
- Kobayashi, N., Cox, D.T., Wurjanto, A., 1991. Permeability effects on irregular wave runup and reflection. *J. Coast. Res.* 7, 127–136.
- Longuet-Higgins, M.S., Stewart, R.W., 1964. Radiation stresses in water waves; a physical discussion, with applications. *Deep Sea Res. Oceanogr. Abstr.* 11, 529–562. [https://doi.org/10.1016/0011-7471\(64\)90001-4](https://doi.org/10.1016/0011-7471(64)90001-4).
- Madsen, P.A., Sørensen, O.R., Schäffer, H.A., 1997. Surf zone dynamics simulated by a Boussinesq type model. Part I. Model description and cross-shore motion of regular waves. *Coast. Eng.* 32, 255–287. [https://doi.org/10.1016/S0378-3839\(97\)00028-8](https://doi.org/10.1016/S0378-3839(97)00028-8).
- Mase, H., 1989. Random wave runup height on gentle slope. *J. Waterw. Port Ocean Eng.* 115, 649–661. [https://doi.org/10.1016/ASCE\)0733-950X\(1989\)115:5\(649](https://doi.org/10.1016/ASCE)0733-950X(1989)115:5(649).
- Medellin, G., Brinkkemper, J.A., Torres-Freyermuth, A., Appendini, C.M., Mendoza, E.T., Salles, P., 2016. Run-up parameterization and beach vulnerability assessment on a barrier island: a downscaling approach. *Nat. Hazards Earth Syst. Sci.* 16, 167–180. <https://doi.org/10.5194/nhess-16-167-2016>.
- Miche, M., 1951. Le pouvoir réfléchissant des ouvrages maritimes. *Ann Ponts Chausées* 121, 285–319.
- Montaño, J.K., Blossier, B., Osorio, A.F., Winter, C., 2019. The role of frequency spread on swash dynamics. *Geo-Marine Lett.* <https://doi.org/10.1007/s00367-019-00591-1>.
- Nicolae Lerma, A., Pedreros, R., Robinet, A., Sénéchal, N., 2017. Simulating wave setup and runup during storm conditions on a complex barred beach. *Coast. Eng.* 123, 29–41. <https://doi.org/10.1016/j.coastaleng.2017.01.011>.
- Nielsen, P., 1988. Wave setup: a field study. *J. Geophys. Res.* 93, 15643–15652. <https://doi.org/10.1029/JC093iC12p15643>.
- Nielsen, P., Hanslow, D.J., 1991. Wave runup distributions on natural beaches. *J. Coast. Res.* 7, 1139–1152. <https://doi.org/10.2307/4297933>.
- O'Grady, J.G., McInnes, K.L., Hemer, M.A., Hoeke, R.K., Stephenson, A.G., Colberg, F., 2019. Extreme water levels for Australian beaches using empirical equations for shoreline wave setup. *J. Geophys. Res. Ocean*. <https://doi.org/10.1029/2018JC014871>.
- van Oorschot, J.H., D'Angremont, K., 1968. The effect of wave energy spectra on wave run-up, in: Proc. In: 11th International Conference on Coastal Engineering. London, UK, pp. 888–900. <https://doi.org/10.1061/9780872620131.057>.
- Paprotny, D., Andrzejewski, P., Terefenko, P., Furmańczyk, K., 2014. Application of empirical wave run-up formulas to the Polish Baltic Sea coast. *Plos One* 9. <https://doi.org/10.1371/journal.pone.0105437>.
- Passarella, M., Goldstein, E.B., De Muro, S., Coco, G., 2018. The use of genetic programming to develop a predictor of swash excursion on sandy beaches. *Nat. Hazards Earth Syst. Sci.* 18, 599–611. <https://doi.org/10.5194/nhess-18-599-2018>.
- Poate, T.G., McCall, R.T., Masselink, G., 2016. A new parameterisation for runup on gravel beaches. *Coast. Eng.* 117, 176–190. <https://doi.org/10.1016/j.coastaleng.2016.08.003>.
- Polidoro, A., Dornbusch, U., Pullen, T., 2014. Wave Run-Up on Shingle Beaches - a New Method. HR Wallingford for Environment Agency.
- Power, H.E., Gharabagi, B., Bonakdari, H., Robertson, B., Atkinson, A.L., Baldock, T.E., 2019. Prediction of wave runup on beaches using gene-expression programming and empirical relationships. *Coast. Eng.* 144, 47–61. <https://doi.org/10.1016/j.coastaleng.2018.10.006>.
- Raubenheimer, B., Guza, R.T., Elgar, S., 2001. Field observations of wave-driven setdown and setup. *J. Geophys. Res.* 106, 4629–4638. <https://doi.org/10.1029/2000JC000572>.
- Ruessink, B.G., Kleinhans, M.G., Van Den Beukel, P.G.L., 1998. Observations of swash under highly dissipative conditions. *J. Geophys. Res.* 103, 3111–3118. <https://doi.org/10.1029/97JC02791>.
- Ruggiero, P., Komar, P.D., McDougal, W.G., Beach, R.A., 1996. Extreme water levels, wave runup and coastal erosion. In: Proc. 25th International Conference on Coastal Engineering. Orlando, USA, pp. 2793–2805. <https://doi.org/10.1061/9780784402429.216>.
- Ruggiero, P., Komar, P.D., McDougal, W.G., Marra, J.J., Beach, R.A., 2001. Wave runup, extreme water levels and erosion properties backing beaches. *J. Coast. Res.* 17, 407–419.
- Ruggiero, P., Holman, R.A., Beach, R.A., 2004. Wave run-up on a high-energy dissipative beach. *J. Geophys. Res.* 109. <https://doi.org/10.1029/2003JC002160>.
- Ruju, A., Lara, J.L., Losada, I.J., 2019. Numerical assessment of infragravity swash response to offshore wave frequency spread variability. *J. Geophys. Res. Ocean*. <https://doi.org/10.1029/2019JC015063>.
- Senechal, N., Coco, G., Bryan, K.R., Holman, R.A., 2011. Wave runup during extreme storm conditions. *J. Geophys. Res.* 116. <https://doi.org/10.1029/2010JC006819>.
- Senechal, N., Coco, G., Bryan, K., Macmahan, J., Brown, J., Holman, R., 2013. Tidal effects on runup in presence of complex 3D morphologies under dissipative surf zone conditions. In: Proc. Coastal Dynamics, pp. 1483–1494.
- Senechal, N., Coco, G., Plant, N., Bryan, K.R., Brown, J., MacMahan, J.H.M., 2018. Field observations of alongshore runup variability under dissipative conditions in the presence of a shoreline sandwave. *J. Geophys. Res. Ocean*. 123, 6800–6817. <https://doi.org/10.1029/2018JC014109>.
- Serafin, A., Ruggiero, P., Barnard, P.L., Stockdon, H.F., 2019. The influence of shelf bathymetry and beach topography on extreme total water levels: linking large-scale changes of the wave climate to local coastal hazards. *Coast. Eng.* 150, 1–17. <https://doi.org/10.1016/j.coastaleng.2019.03.012>.
- Stephens, S.A., Coco, G., Bryan, K.R., 2011. Numerical simulations of wave setup over barred beach profiles: implications for predictability. *J. Waterw. Port Coast Ocean Eng.* 137, 175–181. [https://doi.org/10.1061/\(ASCE\)WW.1943-5460.000076](https://doi.org/10.1061/(ASCE)WW.1943-5460.000076).
- Stockdon, H.F., Holman, R.A., Howd, P.A., Sallenger, A.H., 2006. Empirical parameterization of setup, swash, and runup. *Coast. Eng.* 53, 573–588. <https://doi.org/10.1016/j.coastaleng.2005.12.005>.
- Tomás, A., Méndez, F.J., Medina, R., Jaime, F.F., Higuera, P., Lara, J.L., Ortiz, M.D., Álvarez de Eulate, M.F., 2016. A methodology to estimate wave-induced coastal flooding hazard maps in Spain. *J. Flood Risk Manag.* 9, 289–305. <https://doi.org/10.1111/jfr3.12198>.
- Torres-Freyermuth, A., Pintado-Patiño, J.C., Pedrozo-Acuña, A., Puleo, J.A., Baldok, T.E., 2019. Runup uncertainty on planar beaches. *Ocean Dyn.* <https://doi.org/10.1007/s10236-019-01305-y>.
- Vieira da Silva, G., Gomes da Silva, P., Araujo, R.S., Klein, A.H.F., Toldo, E., 2017. Wave run-up on embayed beaches. Study case: Itapocorí bay, Southern Brazil. *Brazilian J. Oceanogr.* 65, 187–200. <https://doi.org/10.1590/S1679-87592017133706502>.
- Villarroel-Lamb, D., Hammeken, A., Simons, R., 2014. Quantifying the effect of bed permeability on maximum wave runup. In: Proc. of the 19th International Conference on Coastal Engineering. Seoul, Korea, <https://doi.org/10.9753/icce.v34.currents.45>.
- Vousdoukas, M.I., Wziatek, D., Almeida, L.P., 2012. Coastal vulnerability assessment

- based on video wave run-up observations at a mesotidal, steep-sloped beach. *Ocean Dyn.* 62, 123–137. <https://doi.org/10.1007/s10236-011-0480-x>.
- Wright, L.D., Short, A.D., Green, M.O., 1985. Short-term changes in the morphodynamic states of beaches and surf zones: an empirical predictive model. *Mar. Geol.* 62, 339–364. [https://doi.org/10.1016/0025-3227\(85\)90123-9](https://doi.org/10.1016/0025-3227(85)90123-9).
- Yanagishima, S., Katoh, K., 1990. Field observation on wave setup near the shoreline, in: Proc. In: 22nd International Conference on Coastal Engineering. Delft, The Netherlands, pp. 95–108. <https://doi.org/10.9753/icce.v22.%25p>.
- Zijlema, M., Stelling, G., Smit, P., 2011. SWASH: an operational public domain code for simulating wave fields and rapidly varied flows in coastal waters. *Coast. Eng.* 58, 992–1012. <https://doi.org/10.1016/j.coastaleng.2011.05.015>.